JB
Journals.ASM.org

Pangenomic Study of *Corynebacterium diphtheriae* That Provides Insights into the Genomic Diversity of Pathogenic Isolates from Cases of Classical Diphtheria, Endocarditis, and Pneumonia

Eva Trost,[a,b] Jochen Blom,[a,c] Siomar de Castro Soares,[a,d] I-Hsiu Huang,[e] Arwa Al-Dilaimi,[a] Jasmin Schröder,[a] Sebastian Jaenicke,[a,c] Fernanda A. Dorella,[d] Flavia S. Rocha,[d] Anderson Miyoshi,[d] Vasco Azevedo,[d] Maria P. Schneider,[f] Artur Silva,[f] Thereza C. Camello,[g] Priscila S. Sabbadini,[g] Cíntia S. Santos,[g] Louisy S. Santos,[g] Raphael Hirata, Jr.,[g] Ana L. Mattos-Guaraldi,[g] Androulla Efstratiou,[h] Michael P. Schmitt,[i] Hung Ton-That,[e] and Andreas Tauch[a]

Institut für Genomforschung und Systembiologie, Centrum für Biotechnologie, Universität Bielefeld, Bielefeld, Germany[a]; CLIB Graduate Cluster Industrial Biotechnology, Centrum für Biotechnologie, Universität Bielefeld, Bielefeld, Germany[b]; Bioinformatics Resource Facility, Centrum für Biotechnologie, Universität Bielefeld, Bielefeld, Germany[c]; Laboratório de Gentíca Celular e Molecular, Departamento de Biologia Geral, Instituto de Ciências Biológicas, Universidade Federal de Minas Gerais, Pampulha, Belo Horizonte, MG, Brazil[d]; Department of Microbiology and Molecular Genetics, University of Texas Health Science Center, Houston, Texas, USA[e]; Instituto de Ciências Biológicas, Universidade Federal do Pará, Guamá, Belém, PA, Brazil[f]; Faculdade de Ciências Médicas, Universidade do Estado do Rio de Janeiro, Rio de Janeiro, RJ, Brazil[g]; Respiratory and Systemic Infection Laboratory, Health Protection Agency, Microbiology Services Division, Colindale, London, United Kingdom[h]; and Laboratory of Respiratory and Special Pathogens, Division of Bacterial, Parasitic, and Allergenic Products, Center for Biologics Evaluation and Research, Food and Drug Administration, Bethesda, Maryland, USA[i]

Corynebacterium diphtheriae is one of the most prominent human pathogens and the causative agent of the communicable disease diphtheria. The genomes of 12 strains isolated from patients with classical diphtheria, endocarditis, and pneumonia were completely sequenced and annotated. Including the genome of _C. diphtheriae_ NCTC 13129, we herewith present a comprehensive comparative analysis of 13 strains and the first characterization of the pangenome of the species _C. diphtheriae_. Comparative genomics showed extensive synteny and revealed a core genome consisting of 1,632 conserved genes. The pangenome currently comprises 4,786 protein-coding regions and increases at an average of 65 unique genes per newly sequenced strain. Analysis of prophages carrying the diphtheria toxin gene _tox_ revealed that the toxoid vaccine producer _C. diphtheriae_ Park-Williams no. 8 has been lysogenized by two copies of the ω^{tox+} phage, whereas _C. diphtheriae_ 31A harbors a hitherto-unknown tox^{+} corynephage. DNA binding sites of the _tox_-controlling regulator DtxR were detected by genome-wide motif searches. Comparative content analysis showed that the DtxR regulons exhibit marked differences due to gene gain, gene loss, partial gene deletion, and DtxR binding site depletion. Most predicted pathogenicity islands of _C. diphtheriae_ revealed characteristics of horizontal gene transfer. The majority of these islands encode subunits of adhesive pili, which can play important roles in adhesion of _C. diphtheriae_ to different host tissues. All sequenced isolates contain at least two pilus gene clusters. It appears that variation in the distributed genome is a common strategy of _C. diphtheriae_ to establish differences in host-pathogen interactions.

Corynebacterium diphtheriae is an important human pathogen of the genus *Corynebacterium* and the causal agent of the communicable disease diphtheria (85). Classical diphtheria is an upper respiratory tract illness initially characterized by a sore throat, low-grade fever, and an adherent membrane (called a pseudomembrane) on the tonsils, pharynx, and/or nasal cavity (24). The most prominent virulence factor of toxigenic *C. diphtheriae* strains is a potent A-B exotoxin named diphtheria toxin. It inhibits protein biosynthesis by ADP-ribosylation of elongation factor EF-2 and kills susceptible host cells (28). As diphtheria toxin is encoded by corynephages, the toxigenicity of *C. diphtheriae* strains is dependent on their lysogenization by a tox^{+} corynephage (40). Although the *tox* gene is part of the phage genome, the regulation of diphtheria toxin expression is under bacterial control, as the corresponding iron-sensing regulator DtxR is encoded by a gene on the *C. diphtheriae* chromosome. Therefore, transcription of the *tox* gene is directly linked to bacterial iron homeostasis; i.e., low iron concentrations induce the expression of diphtheria toxin (73).

C. diphtheriae was first visualized in stained specimens from pseudomembranes by the bacteriologist Edwin Klebs in 1883 (35), and in 1884, *C. diphtheriae* was isolated by Friedrich Loeffler and shown to be the cause of diphtheria (43). In 1890, Emil von Behring isolated the first diphtheria antitoxin from blood samples of an infected horse (84). A few years later, William H. Park and Anna W. Williams isolated a *C. diphtheriae* strain that produced an unusually large amount of diphtheria toxin, later named the Park-Williams no. 8 (PW8) strain (56). Since 1923, a diphtheria toxoid vaccine has been produced from diphtheria toxin treated with formalin to inactivate the toxicity and to maintain the immunogenicity of the protein (34). *C. diphtheriae* PW8 and derivatives thereof are widely used for the initial production of diphtheria toxin by submerged fermentation, because of their ability to secrete large amounts of toxin into the culture supernatant (31, 52). *C. diphtheriae* PW8 is lysogenized by corynephage ω^{tox+}, which moderately differs in its restriction map from the common β^{tox+} phage (60). The ω^{tox+} phage integrated into two nontandem

Received 6 February 2012 **Accepted** 4 April 2012
Published ahead of print 13 April 2012
Address correspondence to Andreas Tauch, tauch@cebitec.uni-bielefeld.de.
Supplemental material for this article can be found at http://jb.asm.org/.

doi:10.1128/JB.00183-12

attachment sites within the chromosome of *C. diphtheriae* PW8, suggesting that the enhanced toxin synthesis is due to a gene dosage effect of the *tox* gene (59). Another prominent *C. diphtheriae* strain is C7(β)$^{tox+}$, which was introduced into laboratory research on diphtheria in 1953. This strain is based on the originally avirulent *C. diphtheriae* culture no. 770 (17) and was lysogenized experimentally with corynephage β^{tox+} in a study on phage-host relationships of *C. diphtheriae* strains (3). Since then, *C. diphtheriae* C7(β)$^{tox+}$ has been used worldwide as a reference strain for genetic research on iron metabolism and the regulation of *tox* gene expression. An initial genome comparison of *C. diphtheriae* C7(−) and *C. diphtheriae* PW8 based on genomic hybridization showed remarkable differences in the distribution of predicted pathogenicity islands (PAIs) and provided the first insights into the diversity of clinical isolates (31).

Up to now, diphtheria has been very effectively controlled in developed countries by an efficient immunization program (83). However, the disease has made a dramatic return in recent years, in particular within Eastern Europe. The largest outbreak since the advent of mass immunization started within Russia and the newly independent states of the former Soviet Union in the 1990s (12). In 2003, the genome of a clinical isolate related to this outbreak (*C. diphtheriae* NCTC 13129) was sequenced at the Sanger Institute to identify candidate virulence factors besides the toxin itself, like iron transport systems and fimbrial proteins (7).

Although *C. diphtheriae* is of great medical importance and (genetic) research has been performed for more than a century, very little is currently known about the molecular basis of pathogenicity and factors contributing to virulence of nontoxigenic *C. diphtheriae* isolates. In the present study, we extended the genetic knowledge of the species *C. diphtheriae* by performing comparative analysis of the complete genome sequences of isolates from patients with classical diphtheria, endocarditis, or pneumonia. In the following sections, we present the results of this sequencing project and the comparison of 13 genome sequences, including those of the widely used strains *C. diphtheriae* PW8 and *C. diphtheriae* C7(β)$^{tox+}$. These data open the way to describe the genome of *C. diphtheriae* at the species level by pangenomics. The microbial pangenome is defined as the full complement of genes in a bacterial species and comprises the "core genome," containing genes present in all isolates of a species, and the "dispensable genome," containing genes present only in a subset of genomes (48). This global view on the gene content of *C. diphtheriae* provides a more accurate account of features associated with the lifestyle and virulence of a human pathogen (26). Moreover, this pangenomics project provides a novel perspective on the evolution of the human-pathogenic species *C. diphtheriae.*

MATERIALS AND METHODS

Bacterial strains and growth conditions. All *C. diphtheriae* strains sequenced in this study are listed in Table 1. The isolates were provided by the strain collection of the University of Rio de Janeiro State (Rio de Janeiro, Brazil). *C. diphtheriae* PW8 and C7(β)$^{tox+}$ were obtained from the strain collection of the Food and Drug Administration (Bethesda, MD). All *C. diphtheriae* strains were routinely grown at 37°C in brain heart infusion (BHI) broth or on Columbia agar supplemented with 5% sheep blood.

Preparation of chromosomal DNA for genome sequencing. The purification of chromosomal DNA from *C. diphtheriae* was performed as described previously (80). Briefly, 50-ml aliquots of bacterial cultures grown for 48 to 72 h in BHI broth were centrifuged at 4°C and 2,000 × *g* for 20 min. The resulting cell pellets were resuspended in 0.6 ml of Tris-NaCl buffer (10 mM Tris [pH 7.0], 10 mM EDTA, 300 mM NaCl) and transferred to VK01 Precellys lysing tubes. The bacterial cells were lysed by means of a Precellys 24-Dual tissue homogenizer using two cycles of 6,500 rpm for 15 s with an interval of 30 s. The chromosomal DNA was subsequently purified by extraction with phenol-chloroform-isoamyl alcohol (25:24:1) and precipitated with ethanol. For the isolation of chromosomal DNA from *C. diphtheriae* PW8 and C7(β)$^{tox+}$, both strains were grown overnight in 3 ml of BHI medium at 37°C, with shaking. Cells were pelleted by centrifugation at 5,000 × *g* for 5 min, and the supernatant was discarded. The cell pellet was resuspended in phosphate-buffered saline (PBS) containing 10 mg/ml lysozyme and incubated at 37°C for 30 min. Following the incubation, the cells were pelleted as described above and the supernatant was discarded. The cell pellet was resuspended in 25 μl of PBS, and chromosomal DNA was isolated using the MasterPure DNA purification kit (Epicentre Technologies, Madison, WI). DNA concentrations were determined with a Tecan Infinite 200 microplate reader.

Genome sequencing of the selected *C. diphtheriae* strains. Purified genomic DNA from *C. diphtheriae* was sequenced with the Genome Sequencer FLX Instrument and titanium chemistry (Roche Applied Science) using a quarter of a PicoTiter Plate per strain. Single-stranded template DNA libraries were established by using 5 μg of genomic DNA. The preparation of DNA libraries was carried out according to standard protocols from Roche Applied Science. DNA concentrations of the DNA libraries were measured with the Agilent RNA 6000 Nano kit. The resulting genomic DNA sequences were assembled with the Newbler Assembler software (version 2.5.3) using default parameters.

For subsequent gap closure, *in silico* predictions of the contig order were computed by the related reference contig arrangement tool r2cat (30) using the default parameters of the integrated *q*-gram filter and the *C. diphtheriae* NCTC 13129 genome sequence as a reference. Based on a sliding-window approach that determines the position of a contig on the reference genome, all matching regions were displayed in an interactive synteny plot, wherein the contigs were oriented automatically according to their matches (30). The remaining gaps in the genome sequences were closed by PCR strategies using genomic template DNAs and Phusion hot-start high-fidelity DNA polymerase (Finnzymes). The PCR assays were performed according to standard protocols from Finnzymes using 1 M betain for efficient denaturation of DNA secondary structures. All contigs and additional DNA sequences were uploaded into the Consed program (20) to finish the genome sequences of the selected *C. diphtheriae* strains.

Annotation and bioinformatics analysis of the complete genome sequences. Initial automated annotations of the assembled genome sequences of the *C. diphtheriae* strains were performed with the GenDB 2.2 system (49). It combines different gene prediction strategies that were executed by means of REGANOR (42), GLIMMER 2.1 (11), and the CRITICA program suite (2) in conjunction with postprocessing by the RBSfinder tool (69). Functional characterization of the predicted proteins was performed by automated searches in public databases, including Swiss-Prot, TrEMBL, Pfam, TIGRFAM, KEGG, COG, CDD, and Interpro (49). Metabolic pathways were annotated by means of *in silico* reconstructions of metabolic networks with the software CARMEN using metabolic pathway information from the KEGG database and manually curated SBML templates (64). The predicted *C. diphtheriae* proteins were mapped onto the SBML templates using bidirectional best BLASTP hits and the scoring matrix BLOSUM62 with an E-value cutoff of 1 × 10^{-10}. The comparative annotation tool provided by the software EDGAR was used for manual data curation and a consistent annotation of the sequenced *C. diphtheriae* genomes (4). Clustered regularly interspaced short palindromic repeats (CRISPRs) and *cas* genes were detected with the CRISPRFinder tool (23). Secreted proteins were detected with SignalP 4.0 using default settings for Gram-positive bacteria (57). Genomic islands and candidate pathogenicity islands were identified with the pathogenicity island prediction software PIPS (68). For this purpose, PIPS performs a combined analysis based on the presence of the following features: (i)

TABLE 1 Overview of sequenced *C. diphtheriae* strains and general features of the genome sequences

Strain	Origin of strain	Genome size (bp)	No. of genes	No. of singletons	No. of transposases	Types of CRISPRs[a]	GenBank accession no.	Reference(s)
NCTC 13129	Isolated from a diphtheria patient in the United Kingdom, 1997; *tox*$^+$	2,488,635	2,368	124	36	I (7); II (26)	BX248353	6, 8
C7(β)$^{tox+}$	Derivative of the avirulent isolate C7, 1954; widely used laboratory strain; *tox*$^+$	2,499,189	2,350	126	69	I (6)	CP003210	3, 15
PW8	Isolated from a diphtheria patient in New York, 1896; widely used toxoid vaccine producer; *tox*$^+$	2,530,683	2,361	101	79	III (15)	CP003216	56
CDC-E8392	Isolated from a diphtheria patient; originally from the Centers for Disease Control and Prevention; *tox*$^+$	2,433,326	2,270	52	66	III (12)	CP003211	58
31A	Isolated from a diphtheria patient (vaccinated adult) in Rio de Janeiro, 1978; *tox*$^+$	2,535,346	2,402	104	93	I (28)	CP003206	47
241	Isolated from a diphtheria patient in Rio de Janeiro, 1981; *tox* negative	2,426,551	2,260	6	87	I (15); II (4)	CP003207	47
VA01	Isolated from a diphtheria patient in Rio de Janeiro, 1999; *tox* negative	2,395,441	2,196	27	66	I (7)	CP003217	80
HC01	Isolated from a blood sample from a patient with fatal endocarditis in Rio de Janeiro, 1993	2,427,149	2,260	7	82	I (15); II (4)	CP003212	47
HC02	Isolated from a blood sample from a patient with endocarditis in Rio de Janeiro, 1999	2,468,612	2,244	69	77	I (5)	CP003213	58
HC03	Isolated from a blood sample from a patient with endocarditis in Rio de Janeiro, 2000	2,478,364	2,268	35	83	III (42)	CP003214	58
HC04	Isolated from a blood sample from a patient with fatal endocarditis in Rio de Janeiro, 2003	2,484,332	2,280	13	79	III (15)	CP003215	58
INCA 402	Isolated from a bronchial wash specimen from a cancer patient with pneumonia in Rio de Janeiro, 2000	2,449,071	2,235	44	65	III (17)	CP003208	80
BH8	Isolated from an inpatient in Rio de Janeiro; antibiotic-resistant strain	2,485,519	2,375	85	97	I (1)	CP003209	This study

[a] The number of repeats is given in parentheses.

deviation from the mean G+C content, (ii) deviation from the codon usage using Colombo-SIGI-HMM, (iii) prediction of flanking tRNAs based on tRNAscan-SE, (iv) prediction of transposases using HMMER3 and Pfam models, (v) prediction of virulence factors based on mVirDB, and (vi) the absence of the putative islands in nonpathogenic bacteria of related species using Artemis and ACT (68). The genome sequence of the nonpathogenic species *Corynebacterium glutamicum* ATCC 13032 was used as a reference (33).

Comparative genomics and pangenomics. All comparative analyses of the sequenced *C. diphtheriae* genomes were performed with EDGAR software (4). Comparative analysis at the protein level was based on an all-against-all comparison of the predicted proteomes. The algorithm used was BLASTP with the standard scoring matrix BLOSUM62 and an initial E-value cutoff of 1×10^{-5}. All BLAST hits were normalized in relation to the best score possible, i.e., the score of a hit of the query gene against itself (4). By dividing the scores of further hits by this best score, a similarity to the best in percent is obtained, the so-called score ratio value (SRV) that reflects the quality of the hit (41). Two genes were considered orthologous when exhibiting a bidirectional best BLAST hit with single SRVs exceeding the precalculated corynebacterial cutoff of 76 (4). The core genome was calculated, based on this information, as the set of genes that are orthologous in all sequenced *C. diphtheriae* strains. A phylogenetic tree was constructed by aligning all orthologous genes of *C. diphtheriae* and masking nonmatching parts of the alignments. The remaining data were concatenated and used for the calculation of a distance matrix, which provides the input for the neighbor-joining method as implemented in the PHYLIP package (13). All genes of the reference genome *C. diphtheriae* C7(β)$^{tox+}$ were selected as a basis for calculating the pangenome of *C. diphtheriae*. These genes were compared to those of a second *C. diphtheriae* genome, and all nonorthologous genes were added to the pangenome. By iteratively repeating this process for all remaining genomes, the gene composition of the final pangenome was deduced (4). The development of the pangenome in dependence on the number of sequenced genomes was calculated by Heaps' law as proposed previously (76). The relevant parameters κ and γ, as well as the confidence intervals, were estimated using the nonlinear least-squares curve fitting with the statistical computing language R.

Whole-genome alignments of the *C. diphtheriae* sequences were calculated using the software Mauve with default parameters (10). Mauve facilitates the accurate detection of rearrangement breakpoints when genomes have unequal gene contents based on an alignment objective score, called a sum-of-pairs breakpoint score. For comparative analysis of the gene composition of DtxR regulons, DNA motif discovery was performed with a hidden Markov model using previously detected DtxR binding sites (6) as input for the HMMER software suite (14). ClustalW2 (39) was used to align the protein sequences of pilus shaft proteins and their related sortases. Phylogenetic trees of pilin-specific sortases, shaft proteins, tip pilins, and base pilins were generated with the neighbor-joining algorithm using MEGA 4.0 software (72).

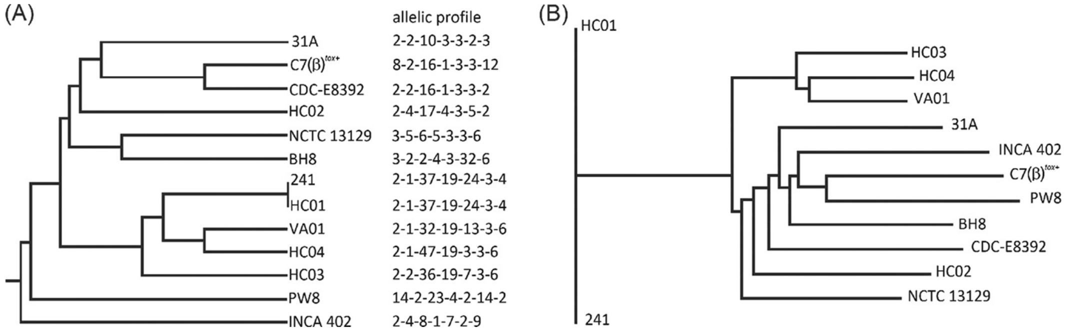

FIG 1 Phylogenetic trees of hitherto-sequenced *C. diphtheriae* strains based on allelic profiles of housekeeping genes (A) and variations in the deduced core genome (B). Allelic profiles of the housekeeping genes were determined according to references deposited in the *C. diphtheriae* MLST database mlstdbNet. The dendrogram was calculated with the PHYLIP package using the unweighted-pair group method with arithmetic mean (UPGMA). The core genome of *C. diphtheriae* was deduced with EDGAR software and includes 1,632 genes. The dendrogram was calculated with the EDGAR system using the neighbor-joining method.

Nucleotide sequence accession numbers. The annotated genome sequences of the *C. diphtheriae* strains have been deposited in the GenBank database with the following accession numbers: C7(β)$^{tox+}$, CP003210; PW8, CP003216; CDC-E8392, CP003211; 31A, CP003206; 241, CP003207; VA01, CP003217; HC01, CP003212; HC02, CP003213; HC03, CP003214; HC04, CP003215; INCA 402, CP003208; and BH8, CP003209.

RESULTS

General features of the sequenced *C. diphtheriae* genomes. In this study, 12 *C. diphtheriae* genomes, including the widely used laboratory strain C7(β)$^{tox+}$ and the prominent toxoid vaccine producer PW8, were sequenced by pyrosequencing with the 454 GS FLX system (Table 1). As infections with *C. diphtheriae* can cause different diseases in humans (29, 50), the strains selected for genome sequencing were originally isolated from patients with classical diphtheria, blood cultures of patients with endocarditis, and a rare case of pneumonia in a cancer patient (Table 1). The sequencing depth of the *C. diphtheriae* genomes ranged from coverages of 29-fold to 55-fold, while the average number of assembled contigs ranged from 33 to 73 (data not shown). After gap closure, the genomic sequences were assembled to circular chromosomes 2.395 Mb (*C. diphtheriae* VA01) to 2.535 Mb (*C. diphtheriae* 31A) in size (Table 1). The average G+C content of each genome is in the range of 53%, which is consistent with the G+C content detected previously in the genome of *C. diphtheriae* NCTC 13129 (7). To ensure consistent annotations of all *C. diphtheriae* genomes, the "comparative annotation function module" of the EDGAR software was used for functional assignments of protein-coding genes (4). Manual annotation of the 12 *C. diphtheriae* chromosomes and concurrent reannotation of the NCTC 13129 genome (9) revealed a median number of 2,294 protein-coding genes for each strain, with the lowest number, 2,196 genes, annotated in the genome of *C. diphtheriae* VA01 and the highest number, 2,402 genes, in the genome of *C. diphtheriae* 31A (Table 1). For the laboratory strain *C. diphtheriae* C7(β)$^{tox+}$, annotation of the 2,499,189-bp chromosome revealed 2,350 protein-coding genes, while the chromosome of the toxoid vaccine producer *C. diphtheriae* PW8 has a size of 2,530,683 bp, with 2,361 predicted protein-coding genes (Table 1).

Phylogenetic tree of the sequenced *C. diphtheriae* strains. To evaluate the relationship of the 13 hitherto-sequenced *C. diphtheriae* strains, a dendrogram based on allelic differences in the following standard set of housekeeping loci (32) was calculated: ATP synthase α chain (*atpA*), DNA polymerase III α subunit (*dnaE*), chaperone protein DnaK (*dnaK*), elongation factor G (*fusA*), 2-isopropylmalate synthase (*leuA*), 2-oxoglutarate dehydrogenase E1 and E2 components (*sucA*), and DNA-directed RNA polymerase β subunit (*rpoB*). Allelic numbers were assigned by performing BLASTN similarity searches against corresponding genes collected in the multilocus sequence typing (MLST) database mlstdbNet (32) and used to deduce a phylogenetic tree with the PHYLIP package (Fig. 1A). *C. diphtheriae* INCA 402, isolated from a pneumonia patient and assigned to the biotype belfanti (82), constituted a distinct subline within the phylogenetic tree, separating it from the other sequenced strains originally isolated from cases of diphtheria and endocarditis. The latter strains show a high degree of genetic diversity, even if they were isolated in the same hospital from patients with similar clinical symptoms, like strains HC01, HC02, HC03, and HC04 (Fig. 1A). The most closely related pair of strains comprises the *tox*-negative isolates *C. diphtheriae* 241 (diphtheria) and *C. diphtheriae* HC01 (endocarditis), which show identical MLST profiles (Fig. 1A).

Another method to determine the phylogenetic relationship of corynebacterial strains is spoligotyping, which is based on arrays of so-called clustered regularly interspaced short palindromic repeats (CRISPRs) (51). These arrays are composed of direct repeats that are separated by nonrepetitive, similar-sized spacers. Together with their associated *cas* genes, CRISPR arrays can confer resistance to phages by RNA interference-like mechanisms (74). Targets for spoligotyping are the spacer regions between the direct repeats, as variations in the number or nucleotide sequence of spacers may provide patterns for the differentiation between subtypes of bacterial isolates (22). Three different types of CRISPR arrays were detected in the genomes of the sequenced *C. diphtheriae* strains (Table 1). CRISPR type I is composed of three *cas* genes (*cas1* to *cas3*), and the number of associated spacers ranged from 1 (*C. diphtheriae* BH8) to 28 (*C. diphtheriae* 31A). The type I CRISPR array was detected in the genomes of eight strains (Table 1). *C. diphtheriae* strains NCTC 13129, 241, and HC01 harbor the additional CRISPR type II, which contains eight *cas* genes (*cas4* to *cas11*). The number of repeats in these arrays ranged from 4 (*C. diphtheriae* 241 and HC01) to 26 (*C. diphtheriae* NCTC 13129). A perfect match of both CRISPR types was detected in the closely related strains *C. diphtheriae* 241 and HC01, as these genomes encode exactly the same CRISPR arrays. CRISPR type III is present

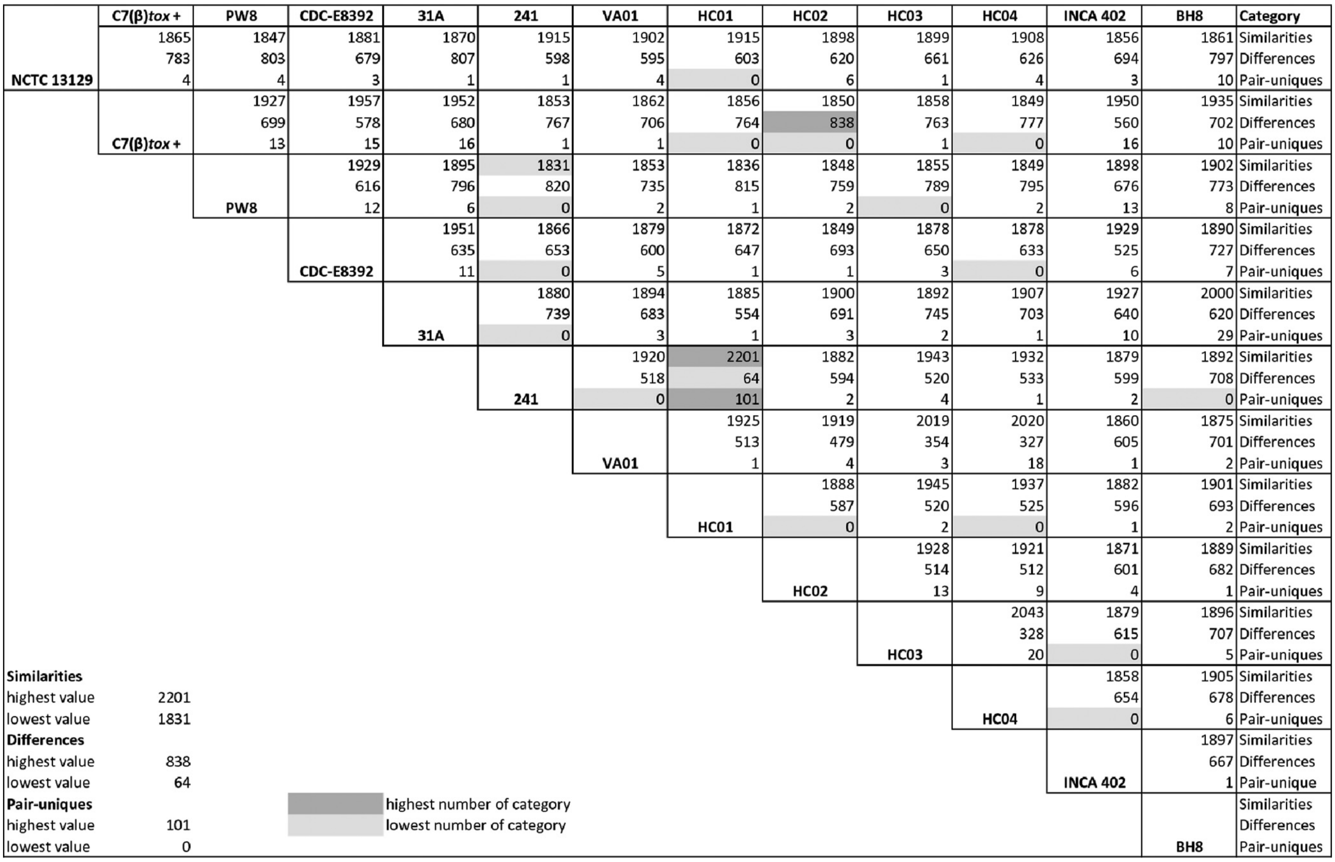

	C7(β)*tox*+	PW8	CDC-E8392	31A	241	VA01	HC01	HC02	HC03	HC04	INCA 402	BH8	Category
	1865	1847	1881	1870	1915	1902	1915	1898	1899	1908	1856	1861	Similarities
	783	803	679	807	598	595	603	620	661	626	694	797	Differences
NCTC 13129	4	4	3	1	1	4	0	6	1	4	3	10	Pair-uniques
		1927	1957	1952	1853	1862	1856	1850	1858	1849	1950	1935	Similarities
		699	578	680	767	706	764	838	763	777	560	702	Differences
	C7(β)*tox*+	13	15	16	1	1	0	0	1	0	16	10	Pair-uniques
			1929	1895	1831	1853	1836	1848	1855	1849	1898	1902	Similarities
			616	796	820	735	815	759	789	795	676	773	Differences
		PW8	12	6	0	2	1	2	0	2	13	8	Pair-uniques
				1951	1866	1879	1872	1849	1878	1878	1929	1890	Similarities
				635	653	600	647	693	650	633	525	727	Differences
			CDC-E8392	11	0	5	1	1	3	0	6	7	Pair-uniques
					1880	1894	1885	1900	1892	1907	1927	2000	Similarities
					739	683	554	691	745	703	640	620	Differences
				31A	0	3	1	3	2	1	10	29	Pair-uniques
						1920	2201	1882	1943	1932	1879	1892	Similarities
						518	64	594	520	533	599	708	Differences
					241	0	101	2	4	1	2	0	Pair-uniques
							1925	1919	2019	2020	1860	1875	Similarities
							513	479	354	327	605	701	Differences
						VA01	1	4	3	18	1	2	Pair-uniques
								1888	1945	1937	1882	1901	Similarities
								587	520	525	596	693	Differences
							HC01	0	2	0	1	2	Pair-uniques
									1928	1921	1871	1889	Similarities
									514	512	601	682	Differences
								HC02	13	9	4	1	Pair-uniques
										2043	1879	1896	Similarities
										328	615	707	Differences
									HC03	20	0	5	Pair-uniques
Similarities											1858	1905	Similarities
highest value	2201										654	678	Differences
lowest value	1831									HC04	0	6	Pair-uniques
Differences												1897	Similarities
highest value	838											667	Differences
lowest value	64										INCA 402	1	Pair-unique
Pair-uniques			▨	highest number of category									Similarities
highest value	101		░	lowest number of category									Differences
lowest value	0											BH8	Pair-uniques

FIG 2 Pairwise comparison of the gene contents of hitherto-sequenced *C. diphtheriae* strains. Similarities denote the number of genes shared by a particular pair of strains, differences display the number of genes not shared within a pair of strains, and pair-uniques correspond to orthologous genes shared only by a distinct strain pair. All calculations were carried out with the software tool EDGAR. The highest and lowest values of each category are listed and specifically marked.

in five *C. diphtheriae* genomes (Table 1), with various numbers of repeats ranging from 12 (*C. diphtheriae* CDC-E8392) to 42 (*C. diphtheriae* HC03). The type III CRISPR array is flanked by eight *cas* genes (*cas12* to *cas19*). The comparison of the identified spacer sequences revealed that only 48 out of the 219 spacers are shared by two or three *C. diphtheriae* strains (data not shown), supporting the view that CRISPR arrays provide a solid basis to discriminate effectively between different *C. diphtheriae* isolates (51).

Pairwise comparison of the sequenced *C. diphtheriae* strains. To obtain more detailed insights into the genetic diversity of the sequenced *C. diphtheriae* strains, the software EDGAR was used to calculate the so-called "similarities" (genes shared by two strains), "differences" (genes not shared by a strain pair), and "pair-uniques" (genes only present in two selected strains) for all possible pairs of strains (Fig. 2). The mean number of similarities between two *C. diphtheriae* strains comprises 1,903 ± 54 orthologous genes, while the mean number of differences comprises 644 genes (with a high standard deviation, ±134), indicating the large variability of the gene content in the selected *C. diphtheriae* strains. The highest number of orthologous genes (i.e., 2,201) and the smallest number of differences (i.e., 64) were calculated for the strain pair *C. diphtheriae* 241 and *C. diphtheriae* HC01 (Fig. 2), supporting their close relationship already observed in the phylogenetic tree based on allelic profiles (Fig. 1A). The highest number of differences (838) was detected in the strain pair *C. diphtheriae* C7β^{tox+} and *C. diphtheriae* HC02, although both belong to the same subline of the phylogenetic tree (Fig. 1A). The lowest number of similarities, with only 1,831 shared genes, was calculated for the strain pair *C. diphtheriae* PW8 and *C. diphtheriae* 241 (Fig. 2), both isolated from patients with classical diphtheria but in different countries and about 100 years apart (Table 1). The number of pair-uniques was strikingly low, with a mean number of five genes shared by only two *C. diphtheriae* strains. The detected sets of pair-uniques mainly comprise genes for transposases or their inactivated derivatives and genes encoding uncharacterized transporters (data not shown). The highest number of pair-uniques (101) was detected in the closely related strains *C. diphtheriae* 241 and *C. diphtheriae* HC01 (Fig. 2). On the other hand, no pair-uniques were detected in 15 pairs of *C. diphtheriae* strains, indicating that the current collection of sequenced genomes largely reflects the gene content of the species *C. diphtheriae*.

For further comparative genomics studies, the annotated protein-coding sequences were grouped into three categories: "core genes" (conserved in all sequenced *C. diphtheriae* strains), "singletons" (genes present in a single strain only), and "distributed genes" (shared by a subset of two or more strains). The bioinformatics analysis of the respective categories provided knowledge of the core genome, strain-specific functions eventually associated with pathogenicity, and the pangenome of the species *C. diphtheriae*.

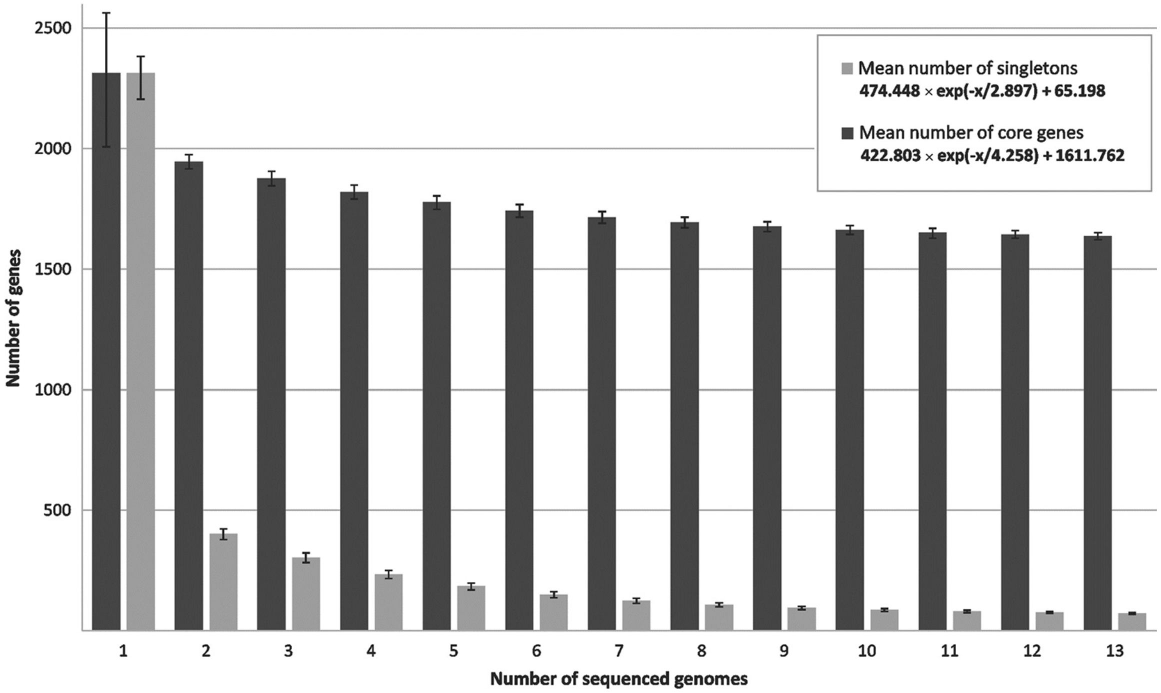

FIG 3 Development of the number of core genes and singletons as a function of the number of sequenced *C. diphtheriae* strains. The respective numbers were calculated for two strains and then iteratively for an increasing number of sequenced genomes, added one by one. The deduced equations denote the exponential decay model based on the median number of core genes and singletons, when increasing numbers of genomes were compared.

Deduced core genome of the species *C. diphtheriae*. The number of core genes of *C. diphtheriae* was determined with the software EDGAR using bidirectional best BLASTP hits with the precalculated score ratio value of 76 as a cutoff. Based on a series of calculations using all genomes individually as a reference, the core genome of the hitherto-sequenced *C. diphtheriae* strains comprises 1,632 genes that are therefore highly conserved in this species. A phylogenetic tree of the *C. diphtheriae* strains was constructed using a concatenated multiple alignment of the detected core genes and a distance matrix, which was calculated with the Kimura algorithm (Fig. 1B). This genome-based approach revealed a different phylogenetic relationship of the 13 *C. diphtheriae* strains compared with the MLST profile (Fig. 1A). The use of a multitude of core genes for genome comparison apparently provided a greater taxonomic resolution of the clinical isolates and showed a close relationship between the widely used strains *C. diphtheriae* PW8 and *C. diphtheriae* C7(β)$^{tox+}$ (Fig. 1B).

To deduce the development of the core genome in dependence on the number of sequenced *C. diphtheriae* strains, the median number of core genes in each genome was calculated based on the permutation of all possible genome comparisons (Fig. 3). These data revealed that the number of core genes is approaching a curve with $422.803 \times e^{(-x/4.258)} + 1{,}611.762$, with *x* being the number of sequenced *C. diphtheriae* genomes and *e* being Euler's number. Hence, the number of core genes present in the species *C. diphtheriae* will comprise about 1,611 protein-coding genes when adding further genome sequences to the current data set. This value revealed a distinct genetic backbone of the species *C. diphtheriae*, which includes approximately 70% of the gene repertoire of the sequenced strains. In other words, about 30% of the gene content of *C. diphtheriae* strains is variable to some extent and therefore belongs to the dispensable portion of the genomes. The number of core genes of *C. diphtheriae* is notably high compared to the previously published corynebacterial backbone of 835 genes calculated with genomic data from the pathogenic and nonpathogenic species *C. diphtheriae*, *Corynebacterium jeikeium*, *Corynebacterium efficiens*, and *C. glutamicum* (86). However, this difference can be explained by the very close relationship of the *C. diphtheriae* isolates belonging to the same corynebacterial species. The core genome of *C. diphtheriae* comprises genes for components of the central carbon and energy metabolism, biosynthesis routes for amino acids, cofactors, purines, and pyrimidines, the basic machineries involved in cell wall formation, DNA replication, DNA repair, transcription, and protein biosynthesis, as well as conserved transcriptional regulatory systems. A remarkably high number of 493 core genes encode proteins with only poorly characterized functions (data not shown).

The highly conserved genomic backbone of the species *C. diphtheriae* was visualized by a whole-genome alignment of the 13 sequenced strains with the software Mauve (Fig. 4). Less conserved areas of the genomes are mostly located around the origin of replication (*oriC*), indicated by the multitude of short conserved blocks interrupted by nonconserved segments (Fig. 4). These genomic areas often include hot spots of insertion sequences and remnants of these elements. Bacterial insertion sequences and their encoded transposases facilitate the formation of DNA inversions, deletions, and replicon fusions, thereby promoting genomic rearrangements (66). A total number of 979 transposase genes were identified in the 13 *C. diphtheriae* genomes (Table 1), representing about 3.3% of the protein-coding regions of an individual strain and probably playing a significant role in genome evolution. The number of transposase genes varied from

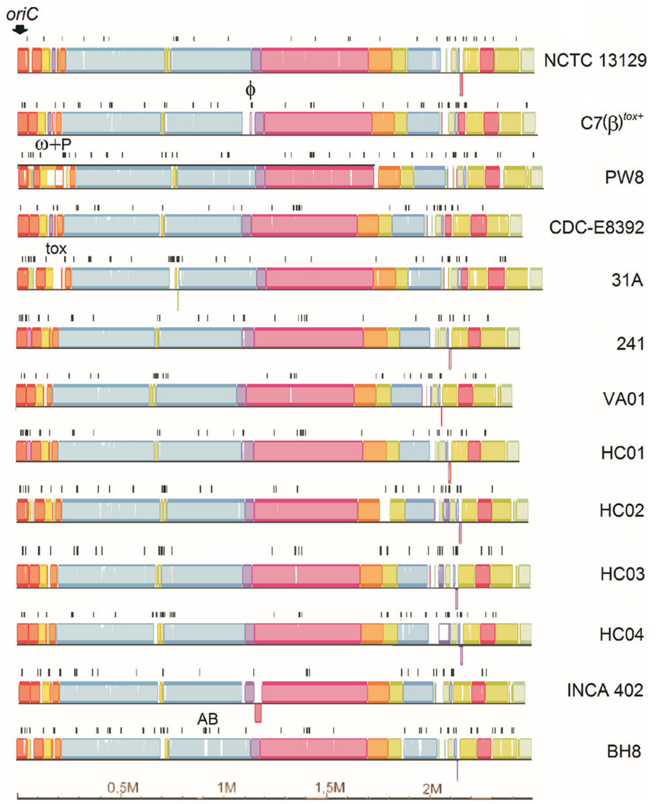

FIG 4 Whole-genome alignment of the 13 sequenced *C. diphtheriae* strains. The nucleotide sequence alignment was calculated with the software Mauve using the genome of *C. diphtheriae* C7(β)$^{tox+}$ as a reference. Each genome is presented in linear view, and homologous DNA segments are shown as colored blocks. The position of the origin of replication (*oriC*) is indicated. Identified transposase genes are marked by black lines. DNA segments mentioned in the text are labeled as follows: ϕ, additional prophage in C7(β)$^{tox+}$; ω+P, ω prophages and adjacent pilus gene cluster in PW8; tox, *tox*$^+$ prophage in 31A; AB, antibiotic resistance gene region in BH8.

65 in *C. diphtheriae* INCA 402 to 97 in the antibiotic-resistant strain *C. diphtheriae* BH8 (Table 1). A nucleotide sequence comparison among the transposase genes revealed a large diversity of mobile elements present in *C. diphtheriae*, as the remarkable number of 413 different insertion sequences was found in the genome data. Most elements are characterized by a low copy number and are present in only a few strains. On the other hand, the ISCod5 element represented by DIP0843 and orthologous genes is distributed in all sequenced *C. diphtheriae* strains, albeit with different copy numbers.

To analyze the correlation between the presence of insertion sequences and less conserved areas of the *C. diphtheriae* genomes, the positions of transposase genes were plotted onto the genome sequences of the 13 *C. diphtheriae* strains (Fig. 4). A preferred integration of insertion sequences around *oriC* and between conserved blocks of core genes was observed in all *C. diphtheriae* genomes. This preference might be due to a gene dosage effect of genes around *oriC* during DNA replication. Previous studies showed that the copy numbers of origin-proximal genes in rapidly growing cells were 2-fold to 4-fold enhanced compared to those of genes flanking the terminus region (67). Mobile elements are also important components facilitating the spread of antibiotic resistance genes by horizontal gene transfer (63). The genome of the antibiotic-resistant isolate *C. diphtheriae* BH8 contains a gene region comprising the known resistance determinants *cmx*, *sul1*, and *tet*(W), probably conferring resistances to chloramphenicol, sulfonamides, and tetracyclines in corynebacteria (65). This gene region is also flanked by insertion sequences, suggesting that it has been acquired by *C. diphtheriae* BH8 via transpositional integration into the chromosome (Fig. 4).

Singletons of the sequenced *C. diphtheriae* strains. The bioinformatics detection of singletons revealed the average number of 61 ± 43 strain-specific genes per sequenced *C. diphtheriae* isolate (Table 1). To characterize the development of the number of singletons in dependence on the number of sequenced *C. diphtheriae* genomes, the median number of strain-specific genes was determined using the permutation of all possible genome comparisons (Fig. 3). The respective calculation indicates that the number of singletons is approaching a curve with $474.448 \times e^{(-x/2.897)} + 65.198$, with x being the number of sequenced *C. diphtheriae* genomes and e being Euler's number. Hence, the median number of singletons estimated to occur in additionally sequenced *C. diphtheriae* isolates comprises about 65 protein-coding genes. The lowest number of singletons was found in the genome of *C. diphtheriae* 241, with only 6 out of the 2,260 annotated genes denoted as strain specific (Table 1). However, the number of singletons in *C. diphtheriae* C7(β)$^{tox+}$ is approximately twice the calculated mean of 65 singletons per additionally sequenced strain, as the highest number of strain-specific genes (126) was detected in this genome. About 61% of these genes were classified as transposases (14 genes) or prophage-related coding regions (63 genes). The respective corynephage integrated into an attachment site within the tRNA^{Leu} gene at about 1.08 Mb on the genomic map of *C. diphtheriae* C7(β)$^{tox+}$ (Fig. 4). The presence of the 57-kb prophage region in the chromosome of *C. diphtheriae* C7(β)$^{tox+}$ was evident from the whole-genome alignment, as it revealed no similarities to the other genomes at the nucleotide level. In principle, the detected prophage singletons are clustered in the *C. diphtheriae* genomes and indicate that different phages or remnants thereof are present in the genomes of the selected strains.

In the case of *C. diphtheriae* PW8, the number of singletons was also above average and calculated as 101 (Table 1). The majority of these genes encode subunits of putative adhesive pili, which play an important role in adhesion of *C. diphtheriae* to host tissues (46). The respective gene cluster is characterized by numerous mobile elements leading to gene disruptions and deletions in this genomic region (CDPW8_0225 to CDPW8_0252). It is located in the immediate vicinity of the duplicated ω prophage harboring the *tox* genes for diphtheria toxin (CDPW8_0179 and CDPW8_0220) and displayed no similarities to any of the other genomes (Fig. 4). This result indicates that singletons may contribute to important strain-specific features which are relevant for the pathogenicity of *C. diphtheriae*.

Deduced pangenome of the species *C. diphtheriae*. The pangenome of a bacterial species includes core genes (conserved in all strains), singletons (strain-specific genes), and distributed genes (48). The latter coding regions are shared by at least two strains and are thus part of the variable gene content of *C. diphtheriae*, in addition to the 793 genes assigned as singletons (Table 1). To calculate the full complement of protein-coding regions in the sequenced *C. diphtheriae* strains, the number of distributed genes was finally determined as 2,361. Accordingly, the sum total of genes included in the pangenome of the sequenced *C. diphtheriae*

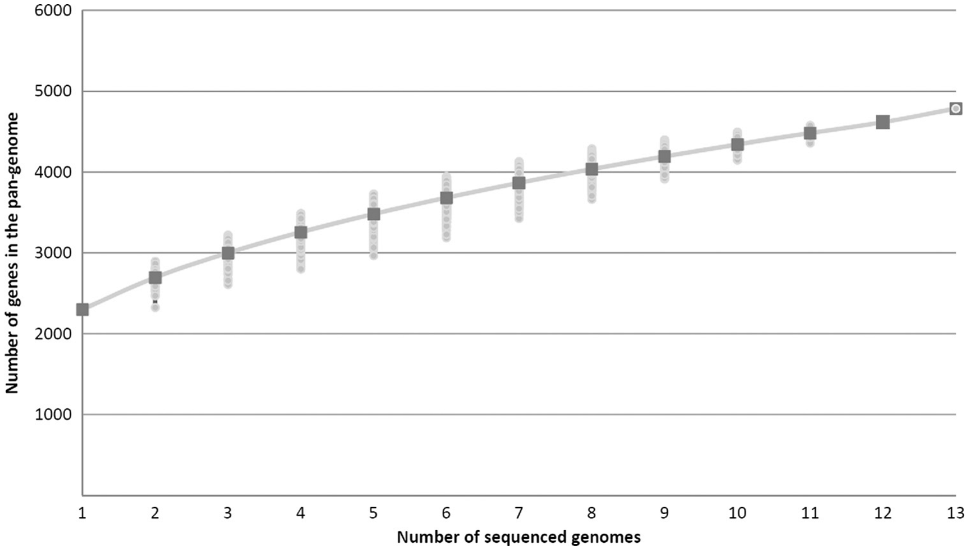

FIG 5 Heaps' law plot representing the development of the pangenome of *C. diphtheriae*. The total number of genes found according to the pangenome analysis is shown for increasing numbers of sequenced *C. diphtheriae* genomes. Medians of the distributions are shown by squares; permutations are indicated.

strains comprises 4,786 genes. This number is about three times the size of the deduced core genome. The further trend of the pangenome size was calculated based on Heaps' law: $n = \kappa \times N^{\gamma}$, with N being the number of sequenced genomes (77). According to the number of genes annotated in the sequenced *C. diphtheriae* genomes, κ was determined as 2,130.67 and γ as 0.306. Hence, the number of genes added to the pangenome with additionally sequenced *C. diphtheriae* strains will increase with an α of 0.69 per newly sequenced genome (Fig. 5). This value is consistent with the continually increasing number of singletons per sequenced strain (Fig. 3) and indicates an open pangenome for the species *C. diphtheriae* (77). A pangenome is considered open when each newly sequenced bacterial strain can be expected to reveal some genes unique within the species, regardless of the number of already-analyzed genomes (25).

Comparison of the sequenced *tox*$^+$ corynephages. Prophages harboring the *tox* gene for diphtheria toxin were identified in *C. diphtheriae* strains C7(β)$^{tox+}$, CDC-E8392, PW8, and 31A, in addition to the *tox*$^+$ prophage known from *C. diphtheriae* NCTC 13129 (Fig. 6). Two copies of corynephage ω^{tox+} were detected in the genome of *C. diphtheriae* PW8, as deduced previously from restriction endonuclease maps of phage DNA (60). The two ω^{tox+} phages are almost identical, as they show only five nucleotide mismatches in their 36-kb genomes. The nontandem copies of the prophage are separated by a 2-kb gene region coding for a putative membrane protein (CDPW8_0180) that is flanked by two copies of a tRNA^{Arg} gene in all *C. diphtheriae* genomes. The tRNA^{Arg} gene located downstream of CDPW8_0180 and its orthologous counterparts usually provide the attachment site *attB* for corynephages ω and β (61). In the case of *C. diphtheriae* PW8, the ω^{tox+} phage integrated into both tRNA^{Arg} genes present on either side of CDPW8_0180, explaining the nontandem arrangement of the prophage genomes. Nucleotide sequence alignments of the identified *tox*$^+$ prophages revealed that the ω^{tox+} phage of *C. diphtheriae* PW8 is homologous to corynephage β^{tox+} that has been integrated into the genome of the previously avirulent strain *C.*

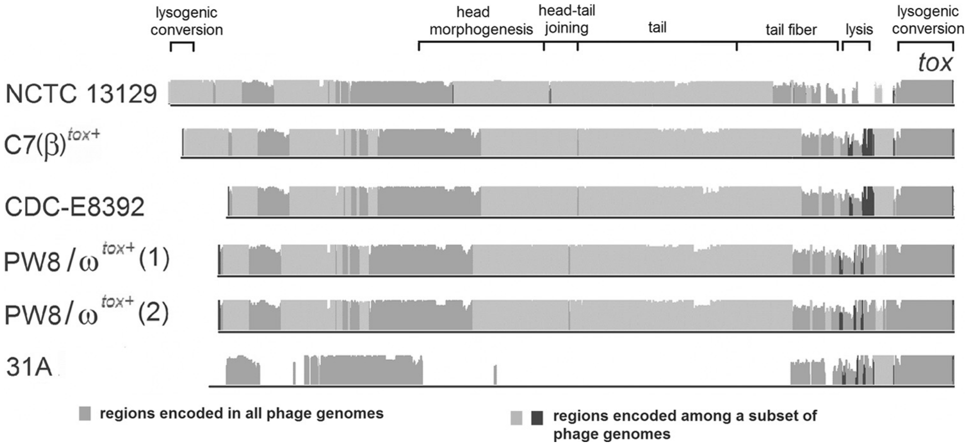

FIG 6 Genome alignment of *tox*$^+$ prophages identified in the sequenced *C. diphtheriae* strains. The nucleotide sequence alignment was calculated with the software Mauve. The height of the plot denotes the similarities of the aligned DNA sequences. The *tox* gene is located at the right-hand end of the prophage genome. The proposed modular structure of the corynephage present in *C. diphtheriae* NCTC 13129 is indicated by annotated brackets.

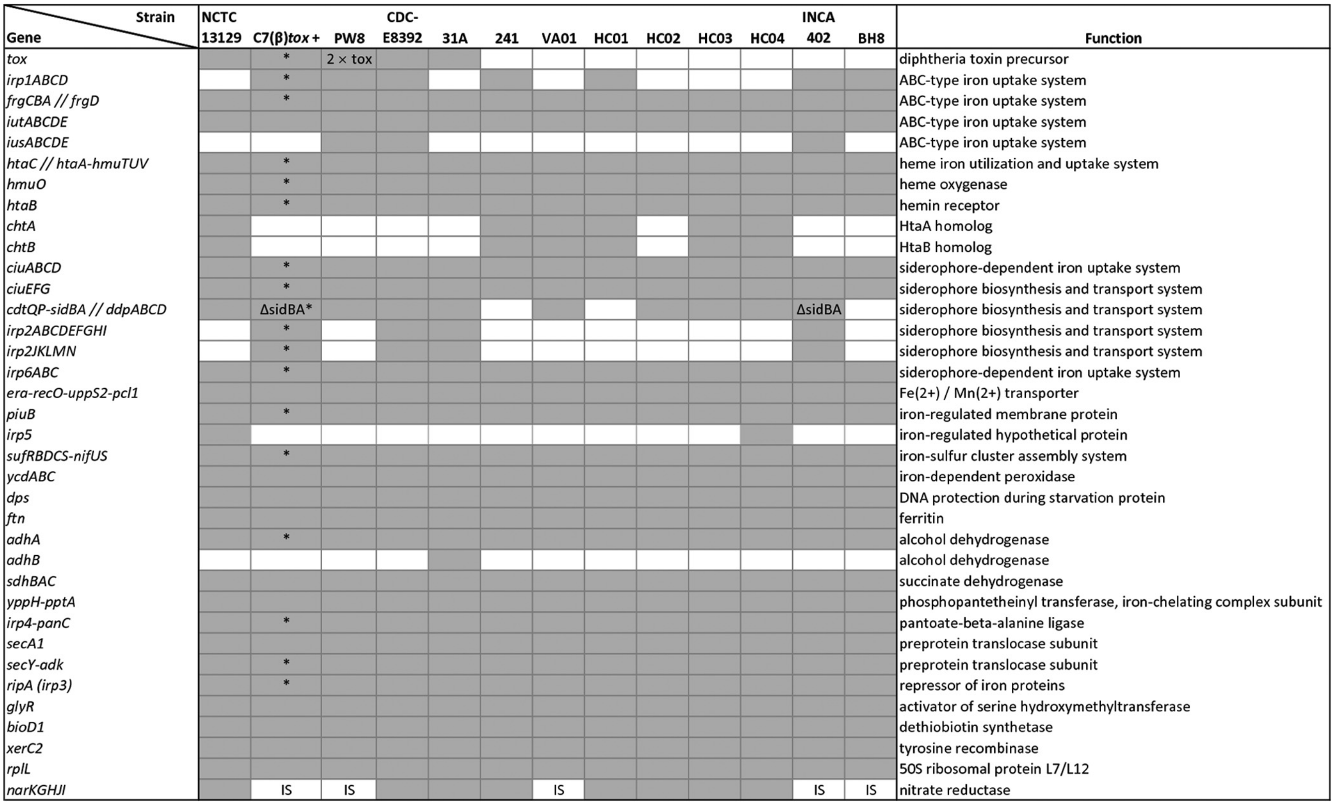

Strain Gene	NCTC 13129	C7(β)*tox*+	PW8	CDC-E8392	31A	241	VA01	HC01	HC02	HC03	HC04	INCA 402	BH8	Function
tox	▨	▨ *	▨ 2 × tox	▨	▨									diphtheria toxin precursor
irp1ABCD		▨ *	▨	▨		▨		▨				▨	▨	ABC-type iron uptake system
frgCBA // frgD	▨	▨ *	▨	▨	▨	▨	▨	▨	▨	▨	▨	▨	▨	ABC-type iron uptake system
iutABCDE	▨	▨	▨	▨	▨	▨	▨	▨	▨	▨	▨	▨	▨	ABC-type iron uptake system
iusABCDE			▨	▨								▨		ABC-type iron uptake system
htaC // htaA-hmuTUV	▨	▨ *	▨	▨	▨	▨	▨	▨	▨	▨	▨	▨	▨	heme iron utilization and uptake system
hmuO	▨	▨ *	▨	▨	▨	▨	▨	▨	▨	▨	▨	▨	▨	heme oxygenase
htaB	▨	▨ *	▨	▨	▨	▨	▨	▨	▨	▨	▨	▨	▨	hemin receptor
chtA	▨					▨	▨	▨		▨	▨			HtaA homolog
chtB	▨					▨	▨	▨		▨	▨			HtaB homolog
ciuABCD	▨	▨ *	▨	▨	▨	▨	▨	▨	▨	▨	▨	▨	▨	siderophore-dependent iron uptake system
ciuEFG	▨	▨ *	▨	▨	▨	▨	▨	▨	▨	▨	▨	▨	▨	siderophore biosynthesis and transport system
cdtQP-sidBA // ddpABCD	▨	▨ ΔsidBA*	▨	▨	▨		▨		▨	▨	▨	▨ ΔsidBA		siderophore biosynthesis and transport system
irp2ABCDEFGHI		▨ *		▨	▨							▨		siderophore biosynthesis and transport system
irp2JKLMN		▨ *		▨	▨							▨		siderophore biosynthesis and transport system
irp6ABC	▨	▨ *	▨	▨	▨	▨	▨	▨	▨	▨	▨	▨	▨	siderophore-dependent iron uptake system
era-recO-uppS2-pcl1	▨	▨	▨	▨	▨	▨	▨	▨	▨	▨	▨	▨	▨	Fe(2+) / Mn(2+) transporter
piuB	▨	▨ *	▨	▨	▨	▨	▨	▨	▨	▨	▨	▨	▨	iron-regulated membrane protein
irp5	▨										▨			iron-regulated hypothetical protein
sufRBDCS-nifUS	▨	▨ *	▨	▨	▨	▨	▨	▨	▨	▨	▨	▨	▨	iron-sulfur cluster assembly system
ycdABC	▨	▨	▨	▨	▨	▨	▨	▨	▨	▨	▨	▨	▨	iron-dependent peroxidase
dps	▨	▨	▨	▨	▨	▨	▨	▨	▨	▨	▨	▨	▨	DNA protection during starvation protein
ftn	▨	▨	▨	▨	▨	▨	▨	▨	▨	▨	▨	▨	▨	ferritin
adhA	▨	▨ *	▨	▨	▨	▨	▨	▨	▨	▨	▨	▨	▨	alcohol dehydrogenase
adhB					▨									alcohol dehydrogenase
sdhBAC	▨	▨	▨	▨	▨	▨	▨	▨	▨	▨	▨	▨	▨	succinate dehydrogenase
yppH-pptA	▨	▨	▨	▨	▨	▨	▨	▨	▨	▨	▨	▨	▨	phosphopantetheinyl transferase, iron-chelating complex subunit
irp4-panC	▨	▨ *	▨	▨	▨	▨	▨	▨	▨	▨	▨	▨	▨	pantoate-beta-alanine ligase
secA1	▨	▨	▨	▨	▨	▨	▨	▨	▨	▨	▨	▨	▨	preprotein translocase subunit
secY-adk	▨	▨ *	▨	▨	▨	▨	▨	▨	▨	▨	▨	▨	▨	preprotein translocase subunit
ripA (irp3)	▨	▨ *	▨	▨	▨	▨	▨	▨	▨	▨	▨	▨	▨	repressor of iron proteins
glyR	▨	▨	▨	▨	▨	▨	▨	▨	▨	▨	▨	▨	▨	activator of serine hydroxymethyltransferase
bioD1	▨	▨	▨	▨	▨	▨	▨	▨	▨	▨	▨	▨	▨	dethiobiotin synthetase
xerC2	▨	▨	▨	▨	▨	▨	▨	▨	▨	▨	▨	▨	▨	tyrosine recombinase
rplL	▨	▨	▨	▨	▨	▨	▨	▨	▨	▨	▨	▨	▨	50S ribosomal protein L7/L12
narKGHJI	▨	IS	IS	▨	▨	▨	IS	▨	▨	▨	▨	IS	IS	nitrate reductase

FIG 7 Comparison of predicted DtxR regulons encoded in the sequenced *C. diphtheriae* genomes. Genes and gene clusters specified by the presence of DtxR binding sites are listed with their proposed physiological functions. The presence of DtxR binding sites is represented by gray boxes. White boxes denote gene clusters and corresponding DtxR binding sites missing in the respective genomes. Specifically marked are the duplication of the *tox* gene in PW8 (2 × tox), the deletion in the *sidBA* gene region (ΔsidBA), and the integration of an insertion sequence into the regulatory region of the nitrate reductase gene cluster (IS). Genes assigned to the same cluster are linked with hyphens. The position of the DtxR binding site is marked by double slashes if it is located between two divergently oriented gene clusters. The asterisks label gene clusters with experimental information on DtxR regulation.

diphtheriae C7 (Fig. 6). This observation confirms an early study demonstrating by restriction mapping that the two phages differ in only three genomic regions (60). Likewise, the prophage detected in *C. diphtheriae* CDC-E8392 is highly similar to corynephage β^{tox+}, whereas the previously reported prophage of *C. diphtheriae* NCTC 13129 shows greater divergence from the nucleotide sequence and gene content of the β^{tox+} phage (Fig. 6).

A remarkably different tox^+ corynephage was detected in the genome of *C. diphtheriae* 31A (Fig. 6). The highest similarity at the nucleotide level to β-like phages is observed at the right-hand end of the prophage genome. This region harbors the diphtheria toxin gene (Fig. 6) and is specified by a decreased G+C content of 42.54%. It is interesting that all *tox* genes detected in this study showed a perfect nucleotide sequence identity, with the exception of a single nucleotide exchange in the respective gene of *C. diphtheriae* CDC-E8392. On the other hand, several proteins encoded by genes in the prophage region of *C. diphtheriae* 31A are homologous to those identified in prophage CULC22IV, which is present in the genome of the closely related *tox*-negative strain *C. ulcerans* BR-AD22. The respective prophage has a size of 41 kb, comprises 53 genes, and has been integrated into a $tRNA^{Thr}$ gene of *Corynebacterium ulcerans* (79). It has been proposed previously that the diphtheria toxin gene was acquired by corynephage β due to the terminal location of *tox* in the genome of the prophage and the significantly decreased G+C content of this gene region (7). The detection of an identical *tox* gene in the prophage of *C. diphtheriae* 31A indicates that the acquisition of the diphtheria toxin gene occurred independently in two different corynephages or that gene shuffling occurred frequently in corynephages.

Variations in gene composition of the iron-dependent DtxR regulons. The diphtheria toxin repressor DtxR of *C. diphtheriae* is known as an iron-dependent regulator that controls the transcription of the diphtheria toxin gene *tox* and a complex gene-regulatory network involved in iron homeostasis (6). In the case of a low iron concentration, DtxR is inactivated and transcription of the *tox* gene is induced (15). As iron is an essential cofactor for proteins involved in important cellular functions, such as respiration and DNA biosynthesis, iron limitation is a common strategy by the mammalian host to suppress bacterial growth (1). Therefore, pathogenic bacteria have to compete for iron in the host to establish an infection, a mechanism that is coupled with the expression of diphtheria toxin in tox^+ strains of *C. diphtheriae* (54). To perform a genome-wide detection of DtxR binding sites, the functional annotations of the *C. diphtheriae* genome sequences were combined with bioinformatics motif searches based on hidden Markov models (6). This approach resulted in the prediction of 36 different DtxR binding sites in the genome sequences of the 13 *C. diphtheriae* strains, of which 26 binding sites were detected in front of highly conserved genes or gene clusters (Fig. 7). These highly conserved parts of the DtxR regulon comprise the diphtheria toxin gene in *tox*$^{+}$ strains and two iron-dependent ABC-type transport systems: the previously described *frgCBAD* genes (38) and the newly identified *iutABCDE* gene cluster. Likewise, genes involved in hemin utilization (*hmuTUV*), the corresponding hemin binding protein genes (*htaABC*), and the *hmuO* gene, which encodes heme oxygenase, are highly conserved (Fig. 7). In addition to the *htaA* and *htaB* genes, several strains feature the *chtA* and *chtB* genes that code for homologs of HtaA and HtaB and also comprise DtxR binding sites in their promoter regions. Likewise, some *C. diphtheriae* strains harbor the DtxR-regulated gene clusters *irp1ABC* and *iusABCDE*, both encoding ABC-type iron uptake systems (Fig. 7).

Moreover, pathogenic bacteria can synthesize and secret high-affinity iron chelators for efficient iron acquisition, termed siderophores (8). Up to now, the *sidBA* genes and the *ciuEFG* gene cluster were assigned functions in siderophore biosynthesis of *C. diphtheriae* (37, 38). The *ciuEFG* gene cluster and the associated siderophore-dependent iron uptake system genes *ciuABCD* are highly conserved parts of the DtxR regulon in all sequenced *C. diphtheriae* strains, while the *sidBA* genes were completely lost in the genomes of *C. diphtheriae* 241, HC01, and BH8 (Fig. 7). The *sidBA* gene region also comprises the *cdtQ* and *cdtP* genes, encoding a permease and an ATPase, respectively. The DtxR binding site of this cluster is located between the *sidB* gene and the *ddpABCD* gene cluster, probably coding for an iron-dependent ABC transport system. Interestingly, the genes *cdtQP* and *ddpABCD* and a remnant of the *sidB* gene including the associated DtxR binding site were found in the genomes of *C. diphtheriae* C7(β)$^{tox+}$ and INCA 402 (Fig. 7). These strains contain an additional gene cluster for siderophore biosynthesis and secretion, which is located downstream of the gene coding for the iron-regulated protein 2 (IRP2). This cluster comprises nine genes, of which the largest coding regions, *irp2C* and *irp2F*, yield amino acid sequence similarities with nonribosomal peptide synthetases from *Burkholderia cenocepacia* PC184 (AAKX00000000) and *Ralstonia solanacearum* IPO1609 (NW_002196568). A putative iron-dependent siderophore uptake system is encoded by the associated *irp2JKLMN* genes. *C. diphtheriae* strains containing all three gene clusters for siderophore biosynthesis and transport are CDC-E8392 and 31A, while the other isolates lack either one or two of the described gene clusters (Fig. 7). Furthermore, the iron-regulated nitrate reductase genes *narKGHJI* are conserved in all sequenced *C. diphtheriae* genomes. The assigned DtxR binding site is depleted by the integration of an insertion sequence located upstream of the gene cluster in the genomes of C7(β)$^{tox+}$, PW8, VA01, INCA 402, and BH8 (Fig. 7). Accordingly, the reconstruction and comparison of DtxR regulons participating in iron homeostasis of *C. diphtheriae* led to the detection of variations in gene composition due to gene gain, gene loss, partial gene deletion, and DtxR binding site depletion.

Distribution and gene content of genomic islands. Further factors besides the *tox* gene are apparently important for the virulence of *C. diphtheriae*, as invasive infections caused by nontoxigenic strains have been increasingly reported over the past years (19). Additional virulence factors can be encoded in genomic islands (GEIs) of the *C. diphtheriae* genome, which often show characteristics of horizontal gene transfer (7). The recently developed software PIPS was used for the detection of GEIs in the sequenced *C. diphtheriae* strains (68). In total, 57 GEIs were identified in the 13 *C. diphtheriae* genomes (see Table S1 in the supplemental material). Comparative content analysis of the detected GEIs revealed that some islands are strain specific, whereas others are completely or partially conserved in more than one strain. Eight GEIs can be regarded as highly conserved in all *C. diphtheriae* genomes (Fig. 8). According to the predicted gene content, the GEIs can be classified as pathogenicity islands, resistance islands, phage islands, or metabolic islands. Many GEIs (19 out of 57) assigned as phage islands encode typical phage products, and the respective regions of the *C. diphtheriae* genomes can be regarded as remnants of prophages. GEIs encoding proteins involved in specific metabolic pathways were assigned as metabolic islands of the *C. diphtheriae* genome. GEI48, for instance, carries genes involved in the degradation of 3-hydroxyphenylpropionic acid to succinate, pyruvate, and acetaldehyde, whereas other metabolic islands encode enzymes involved in polysaccharide degradation (GEI04) or components of sugar transport systems (GEI41). The majority of the resistance determinants of *C. diphtheriae* are encoded by genes located within GEI32, GEI38, and GEI54. These genomic islands encode proteins for heavy metal ion resistance, such as cadmium, copper, mercury, and arsenic resistance, and the clustered antibiotic resistance determinants in the genome of *C. diphtheriae* BH8.

The detected GEIs also include the previously identified pathogenicity islands (PAIs) of *C. diphtheriae* NCTC 13129 (Fig. 8). These PAIs comprise the β^{tox+} prophage region (GEI01), the *spaDEF* (GEI02) and *spaABC* (GEI10) gene clusters encoding adhesive pili, and the *cdtQP-sidBA-ddpABCD* gene cluster for siderophore biosynthesis and transport (GEI12) (7). Moreover, the software PIPS detected additional PAIs in the genome of *C. diphtheriae* NCTC 13129, including the *irp6ABC* genes for a siderophore-dependent iron uptake system (GEI15) and the second siderophore biosynthesis and transport gene cluster, *ciuABCDEFG* (GEI19). The search for pathogenicity islands in the genomes of *C. diphtheriae* led to the detection of 10 additional islands not present in strain NCTC 13129. These PAIs include the third siderophore biosynthesis and transport gene cluster, i.e., *irp2* (GEI26), additional iron transport systems (GEI34, GEI 36, GEI37, and GEI42), a collagen adhesion protein gene (GEI27), and additional gene clusters for adhesive pili (GEI30, GEI47, GEI49, and GEI52). Therefore, the extended search for PAIs in the genomes of the sequenced *C. diphtheriae* strains revealed new gene clusters with characteristics of horizontal gene transfer, which are probably involved in iron acquisition and the formation of adhesive pili.

Conservation and heterogeneity of pilus gene clusters in *C. diphtheriae* clinical isolates. Adhesive pili play pivotal roles in bacterial colonization, pathogenesis, and biofilm development (45). Pilus assembly in corynebacteria occurs by a two-step mechanism, whereby pilins are polymerized and then covalently anchored to cell wall peptidoglycan (62). In *C. diphtheriae*, a pilin-specific sortase catalyzes the polymerization of the pilus, consisting of the shaft protein, tip pilin, and base pilin (45). By amino acid sequence homology and BLASTP searches using the pilin motif and cell wall sorting signal as queries, we identified at least two pilus gene clusters in each of the sequenced genomes from 12 *C. diphtheriae* clinical isolates, with *C. diphtheriae* HC04 harboring four pilus gene clusters (Fig. 9). To designate each pilin according to known pilins of the reference strain *C. diphtheriae* NCTC 13129, ClustalW2 was employed to align the protein sequences for pilus shaft proteins and their cognate sortases. Their phylogenetic trees were then reconstructed with the neighbor-

	NCTC 13129	C7(β)tox +	PW8	CDC-E8392	31A	241	VA01	HC01	HC02	HC03	HC04	INCA 402	BH8
GEI01	10	6	20	6	2	0	0	0	0	0	0	0	0
GEI02	10	3	3	5	3	5	3	5	5	3	6	5	3
GEI03	10	10	10	10	10	10	10	10	10	10	10	10	10
GEI04	10	4	4	4	3	2	7	2	5	7	8	3	5
GEI05	10	10	10	10	10	10	10	10	10	10	10	10	10
GEI06	10	2	3	3	3	3	7	3	8	6	6	3	4
GEI07	10	1	1	1	1	3	1	3	1	4	1	3	1
GEI08	10	2	2	2	2	8	2	8	2	2	2	3	2
GEI09	10	1	1	1	1	1	1	1	1	1	1	1	4
GEI10	10	0	5	6	0	8	8	8	10	10	20	0	5
GEI11	10	3	2	3	4	7	5	7	7	5	6	2	4
GEI12	10	5	6	6	7	3	6	3	7	6	6	6	3
GEI13	10	1	0	0	0	8	3	8	0	3	4	0	0
GEI14	10	6	3	3	6	5	6	5	5	3	3	4	6
GEI15	10	6	2	6	5	5	6	5	6	6	6	6	5
GEI16	10	10	10	10	10	10	10	10	10	10	10	10	10
GEI17	10	10	10	10	10	10	10	10	10	10	10	10	6
GEI18	10	8	5	5	5	8	6	8	8	6	6	8	10
GEI19	10	7	8	9	9	9	8	9	9	8	7	8	8
GEI20	10	6	8	6	6	10	10	10	10	9	10	6	8
GEI21	10	4	6	4	4	4	7	4	6	5	20	4	4
GEI22	10	8	8	8	9	8	9	8	9	9	9	8	8
GEI23	10	8	8	7	8	7	7	7	7	6	8	8	8
GEI24	1	10	0	0	1	1	0	1	0	0	0	0	1
GEI25	3	10	8	8	9	4	5	4	4	8	4	9	8
GEI26	1	9	1	5	6	1	1	1	1	1	1	5	0
GEI27	0	10	0	1	1	1	0	1	0	0	0	0	0
GEI28	2	10	2	3	5	1	2	1	2	2	2	3	5
GEI29	3	3	10	8	3	3	3	3	3	9	9	8	3
GEI30	1	1	10	1	1	2	2	2	1	2	1	1	2
GEI31	0	8	10	0	0	0	0	0	0	1	0	0	6
GEI32	1	5	10	3	2	1	1	1	2	0	1	1	3
GEI33	2	2	10	2	2	2	2	2	2	2	2	2	2
GEI34	0	0	10	4	1	0	0	0	0	0	0	2	0
GEI35	5	6	10	5	5	5	6	5	7	5	5	9	6
GEI36	0	5	0	10	2	1	0	1	0	0	0	2	1
GEI37	1	6	1	10	5	1	1	1	1	1	1	5	1
GEI38	3	4	4	4	10	4	3	4	8	4	4	4	8
GEI39	2	3	2	3	10	0	0	0	0	0	0	0	0
GEI40	2	1	1	1	10	2	1	2	1	2	1	1	1
GEI41	0	3	0	1	10	0	1	0	0	1	1	0	7
GEI42	3	3	1	3	4	10	3	9	3	4	4	3	4
GEI43	0	0	1	0	0	10	0	6	0	0	0	2	0
GEI44	2	2	2	2	1	2	10	2	2	1	8	2	2
GEI45	0	0	0	0	0	0	0	0	10	0	0	0	0
GEI46	3	2	2	2	2	2	3	2	10	5	6	3	3
GEI47	2	4	2	3	4	2	4	2	2	10	4	2	5
GEI48	2	1	1	1	1	3	2	3	2	10	5	1	3
GEI49	2	0	0	0	1	4	6	4	0	10	6	0	1
GEI50	5	4	6	4	4	4	6	4	6	10	5	6	4
GEI51	2	3	1	1	1	7	2	6	4	3	1	10	2
GEI52	5	8	5	5	8	5	5	5	8	5	5	10	5
GEI53	2	2	6	6	2	2	2	2	2	2	2	10	2
GEI54	3	4	5	4	3	3	4	3	4	3	3	10	4
GEI55	0	0	0	0	0	0	0	0	0	0	0	0	10
GEI56	3	3	3	3	4	4	3	4	3	2	3	4	10
GEI57	3	7	5	6	3	5	3	5	3	3	3	6	10

Legend:

0	0-10%
1	10-20%
2	20-30%
3	30-40%
4	40-50%
5	50-60%
6	50-60%
7	60-70%
8	70-80%
9	80-90%
10	90-100%
20	The whole island is duplicated

FIG 8 Genomic islands detected in the sequenced *C. diphtheriae* genomes and comparison of the predicted gene contents. The genomic islands were identified with the software PIPS, and the deduced similarities are shown as percentages.

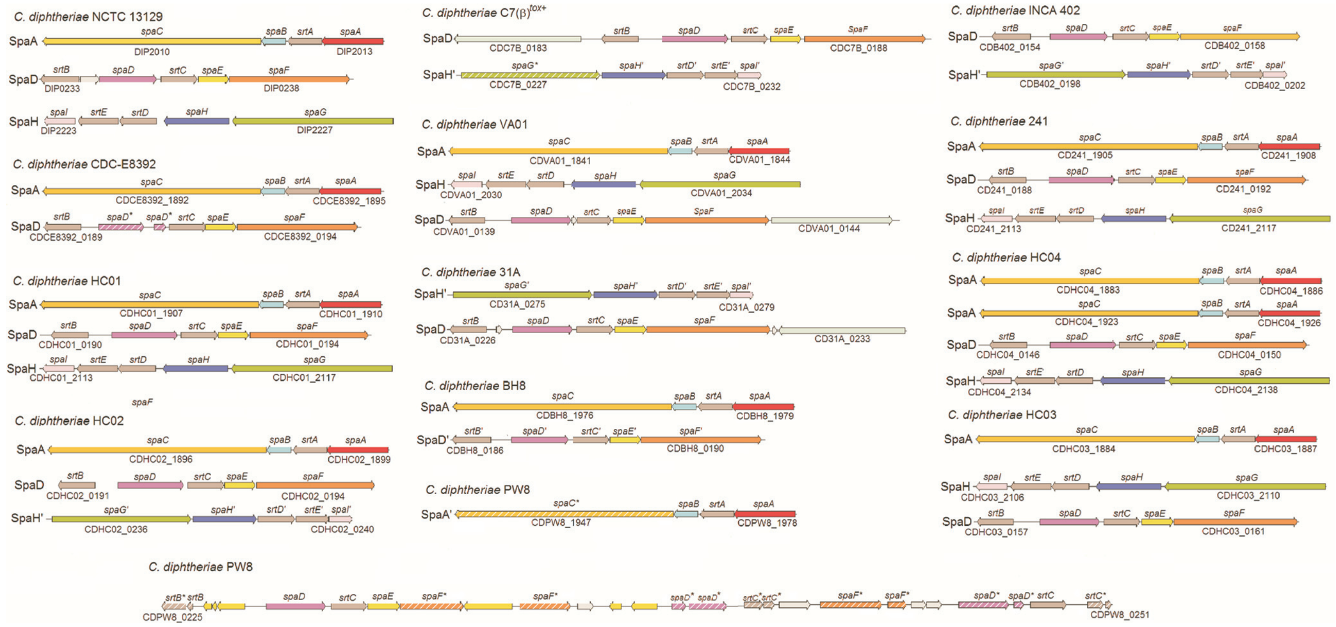

FIG 9 Overview of pilus gene clusters found in the sequenced *C. diphtheriae* strains in relation to the reference strain *C. diphtheriae* NCTC 13129. Homologous pilin genes are indicated by color; sortase genes are shown in dark gray. Genes encoding hypothetical proteins in the pilus gene cluster of *C. diphtheriae* PW8 are shown in light gray; mobile elements are labeled in yellow. Genes similar to SpaD and SpaH types are denoted with primes. Asterisks and hatched arrows indicate fragmented genes.

joining algorithm using MEGA 4.0 (72); similarly, the phylogenetic trees of minor pilins were produced. Built on these analyses, we assigned each pilus gene cluster according to the pilus shaft protein, i.e., SpaA, SpaD, or SpaH type (Fig. 9). Although SpaA pilus gene clusters were found in 9 out of 12 strains, with *C. diphtheriae* HC04 harboring two SpaA loci, namely, SpaA1 and SpaA2, SpaA pilins are mostly conserved (Fig. 10). Interestingly, SpaD pilins are the most divergent group among the three types of shaft proteins (Fig. 10) and found in all 12 strains (Fig. 9). Only a few *C. diphtheriae* strains harbor the SpaH-type gene clusters, and they appear to form two clades in the phylogenetic tree, i.e., SpaH and SpaH′ type (Fig. 9 and 10).

Significantly, cognate pilin-specific sortases display the same trend, with sequences of pilin-specific sortase SrtA for SpaA highly conserved (Fig. 9 and 10). As expected, pilin-specific sortases for SpaD pili (SrtB and SrtC) are the most divergent enzymes, followed by the cognate sortase enzymes for the SpaH pili (SrtD and SrtE). Intriguingly, while all tip pilin SpaC homologs are greatly conserved, the tip pilins for the other pilus types are varied (Fig. 11). The majority of SpaF homologs form a clade that is closer to SpaC homologs, but they are much different from two clades of SpaG pilins, one of which is extremely conserved (Fig. 11). A second SpaF-like tip protein is encoded as part of the SpaD-type clusters in *C. diphtheriae* VA01 and 31A. With the exception of *C. diphtheriae* BH8, the base SpaB pilins are mostly conserved, and the same is true for SpaI pilins, which are present in only a few isolates (Fig. 11). As anticipated, the base pilins for the SpaD-type pili, i.e., SpaE pilins, are also highly divergent (Fig. 11). Of note, SpaE pilin of the vaccine strain *C. diphtheriae* PW8 is closer to SpaI homologs. It is also noteworthy that *C. diphtheriae* PW8 contains a degenerated SpaD gene cluster with multiple intact and disrupted genes encoding SpaD, SpaE, and SpaF pilins and sortases SrtB and SrtE (Fig. 9), in addition to a SpaA locus with a disrupted *spaC* gene (31). Sequences of mobile DNA elements are also detected in the SpaD locus of *C. diphtheriae* PW8, suggesting horizontal gene transfer for gene duplication.

DISCUSSION

The concept of the pangenome was introduced into genomic research by Tettelin and coworkers in 2005 and defined as the full complement of genes in a bacterial species consisting of the core genome and the dispensable genome (75). The core genome contains all genes present in a collection of analyzed strains of a bacterial species, defines the major phenotypic traits of an organism, and is essential for basic cellular functions, such as growth and reproduction or maintenance and survival (53). The variability of genome sizes of different strains is caused by the dispensable genome, which significantly contributes to the diversity of a bacterial species and provides pathways or functions which can confer selective advantages involved in strain-specific niche adaptations (16, 48). The dispensable genome is mainly based on the gene pool available for inclusion into the bacterial genome by mechanisms of horizontal gene transfer (48). Moreover, genome reduction by gene loss, genome rearrangements, and expansion of functional capabilities through gene duplication are forces that have shaped the microbial genome during its evolution (16). In general, the bacterial pangenome can be classified as closed or open (77). A pangenome is considered to be closed if the number of new genes added per newly sequenced genome converges to zero. Therefore, a closed pangenome indicates a static genomic content that is no longer expendable by genome sequencing. It is thus possible to acquire the full gene pool of such a bacterial species by adding a sufficient number of sequenced genomes. A recent systematic study on the pangenomes of 34 bacterial species demonstrated that one-third of the considered microorganisms have a closed pangenome, including the two actinobacteria *Bifidobacterium*

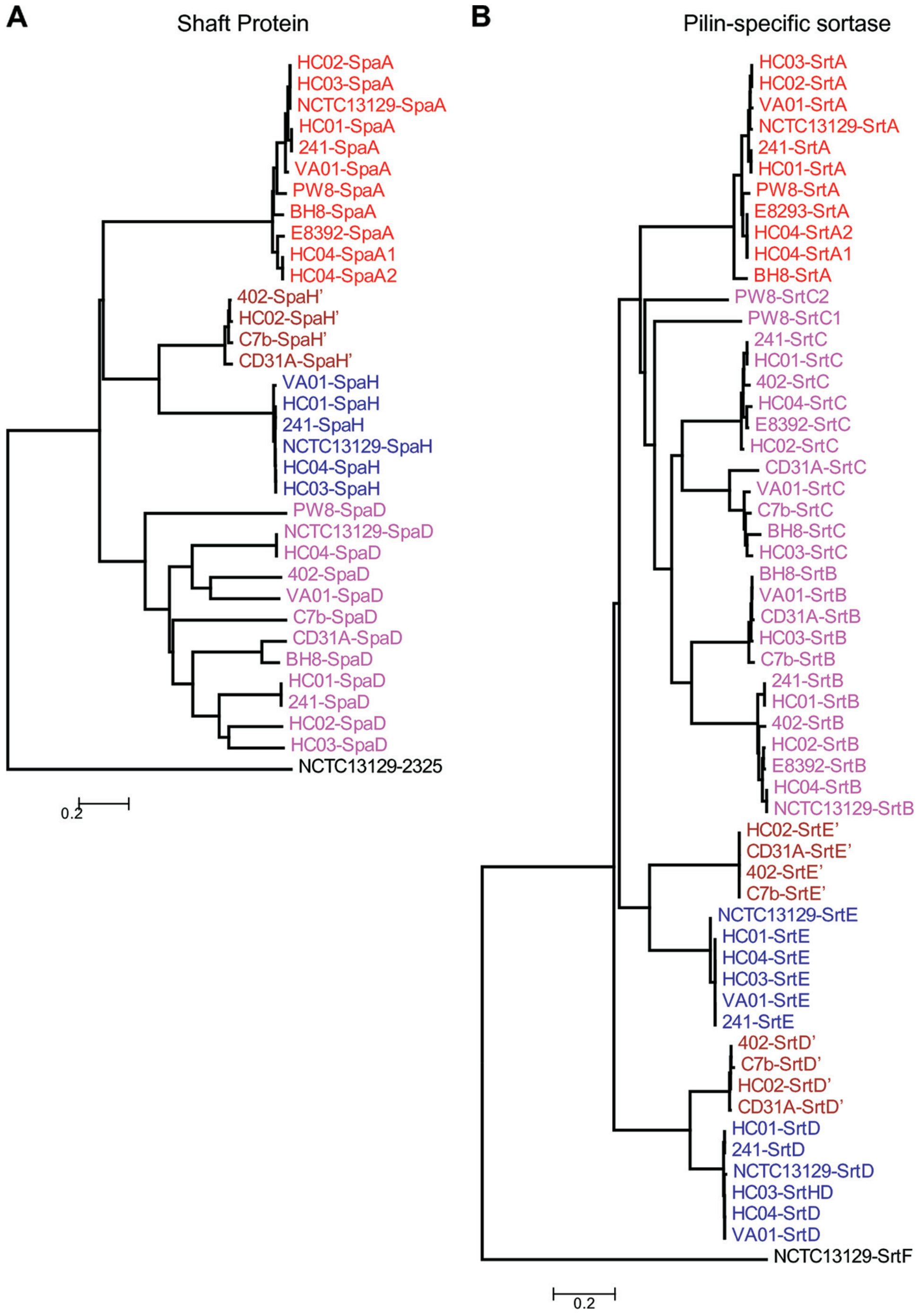

FIG 10 Analysis of pilus shaft proteins (A) and the corresponding sortases (B). ClustalW2 was used to align the protein sequences for major pilin subunits and the predicted sortases of 13 *C. diphtheriae* strains. Their phylogenetic trees were reconstructed with the neighbor-joining algorithm using MEGA 4.0 software. Locus tags are color-coded to indicate the pilus types of the reference strain *C. diphtheriae* NCTC 13129. Proteins similar to SpaH, SrtD, and SrtE are denoted with primes.

animalis and *Mycobacterium tuberculosis* (5, 25). A pangenome is classified as open if new genes were recognized with newly sequenced genomes of a bacterial species (77). An open pangenome is associated with dynamic gene content and was previously calculated for the actinobacterium *Bifidobacterium longum* (5). The present study compares the gene contents of 13 *C. diphtheriae* genomes, including the widely studied strains *C. diphtheriae* PW8 and *C. diphtheriae* C7(β)$^{tox+}$. Calculating the development of the corynebacterial gene content according to Heaps' law, the pangenome of *C. diphtheriae* was classified as open. The mean number of newly detected genes per genome is particularly low when considering the spectrum of countries, different diseases, and the points in time the sequenced *C. diphtheriae* strains were isolated. This result suggests that the calculated pangenome with its present

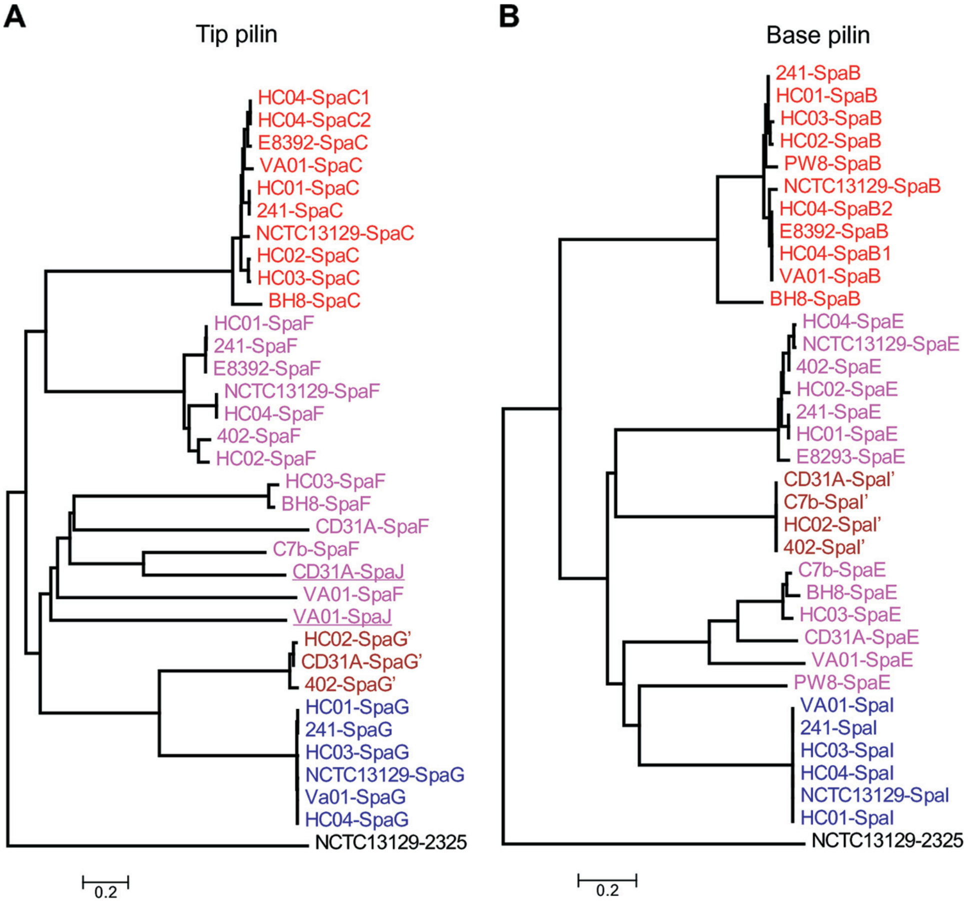

FIG 11 Phylogenetic trees of the tip (A) and base (B) pilus proteins. ClustalW2 was used to align the protein sequences for tip and base pilins of 13 *C. diphtheriae* strains. Phylogenetic trees were reconstructed with the neighbor-joining algorithm using MEGA 4.0 software. Locus tags are color-coded to indicate the pilus types of the reference strain *C. diphtheriae* NCTC 13129. Proteins similar to SpaG and SpaI are denoted with primes.

gene content largely reflects the genetic diversity of the species *C. diphtheriae*. Differences in the gene contents of *C. diphtheriae* strains were mainly found in genomic islands located around the origin of replication and showing several characteristics of horizontal gene transfer (68). The specific location of genomic islands could be related to structural constraints of the bacterial chromosome or the accessibility of different chromosomal regions to foreign DNA elements such as insertion sequences. The detected genomic islands are embedded in a highly stable genomic backbone accounting for 70% of the gene content of *C. diphtheriae*. This profound stability of the core genome is characteristic of corynebacterial species lacking recombination enzymes generally involved in genomic rearrangements (81). The absence of these enzymes in *C. diphtheriae* prevents a rapid evolution of the core genome by recombination and suggests that intraspecific differences are probably related not to a large extent to variations in the genome's architecture but to differences in the distinct gene repertoires of different strains. The detected genomic islands account significantly for the genetic diversity of *C. diphtheriae*, as the dispensable genome constitutes about 30% of the gene content of each strain. A comprehensive comparative work on the open pangenome of *E. coli* estimated a core genome of 1,472 conserved gene families and a pangenome of 13,296 gene families comprising the full complement of genes (44). Some of these variable genes tend to be colocalized on genomic islands of the *E. coli* chromosome. In contrast to *C. diphtheriae*, the variable gene content of this enterobacterial species makes up more than 90% of the pangenome (44).

A marked difference between the *C. diphtheriae* strains is the presence of *tox*$^+$ prophages that were identified in five genome sequences. Analysis of the prophage regions revealed that the ω^{tox+} phage of *C. diphtheriae* PW8 is homologous to the common β^{tox+} phage but present twice as a nontandem repeat. These genome data confirm a previous report, suggesting a second integration of the *tox*$^+$ corynephage and thus a gene dosage effect as a cause for the high-level synthesis of diphtheria toxin in *C. diphtheriae* PW8 (59). Moreover, the genomic sequences revealed the presence of a new *tox*$^+$ corynephage that was identified in the genome of *C. diphtheriae* 31A. The genome sequence of the prophage shows similarities to the β^{tox+} corynephage and the cryptic prophage ϕCULC22IV from *C. ulcerans* BR-AD22 (79). Extensive similarity to the β^{tox+} phage was observed in the *tox* gene region, whereas the components of the basic phage machinery are more similar to ϕCULC22IV. This result indicates that the genome architecture of *tox*$^+$ corynephages is more diverse and that additional phages contribute to the spread of the *tox* gene in the human population. Diversity of the gene repertoire was also detected in regulons contributing to iron homeostasis in *C. diphtheriae*, including genes for iron transport systems, iron-dependent proteins, and the diphtheria toxin. These variations are based on differences in gene composition due not only to gene gain or gene loss but also to the depletion of DNA binding sites for the responsible regulator DtxR. As iron plays a vital role in bacterial infections due to its restricted availability in the host and functions as major environmental signal, proteins involved in iron acquisition are recognized as essential virulence factors during the infection of a mammalian host (21). Therefore, variations in the regulatory network of DtxR might lead to differences in iron supply of the bacterial cell, thereby influencing the expression of the *tox* gene and the virulence of the *C. diphtheriae* strains.

A remarkable outcome of this study is the detection of a great variety of pilus gene clusters encoding adhesive pili in *C. diphtheriae*. The pilin gene clusters of the tox^+ isolate *C. diphtheriae* NCTC 13129 were intensely studied in recent years (18, 71, 78). It was demonstrated that the assembly process depends on pilin-specific sortases as well as the housekeeping sortase and that the SpaA-type pilus is necessary for the specific adherence of *C. diphtheriae* to human pharyngeal epithelial cells (46, 70). The protein components of the pilus, i.e., shaft protein, tip pilin, and base pilin, showed a great diversity in their amino acid sequences, and most of their encoding genes were assigned as singletons during the pangenome analysis. This result implies that important variations exist on the cell surface of toxigenic and nontoxigenic *C. diphtheriae* strains that are relevant for the initial step of an infection. Different degrees of attachment of *C. diphtheriae* strains to HEp-2 cell monolayers were reported previously (27). Differences in adhesion of *C. diphtheriae* C7(−) and *C. diphtheriae* PW8 to Detroit 562 cells were also reported, and PW8 showed a reduced level of adherence compared with C7(−) (29). Mutations in the base pilin SpaB and the tip pilin SpaC of the SpaA-type pilus were shown to reduce the adhesive activity of *C. diphtheriae* (46). In *C. diphtheriae* PW8, the *spaC* gene is characterized by a frameshift mutation (31), and almost all genes of the complex SpaD pilus gene cluster of PW8 are apparently inactivated by transpositional integration of insertion sequences. However, factors other than pili can contribute to cell adhesion of *C. diphtheriae*, including members of the resuscitation-promoting factor-interacting protein family (DIP1281) and the cell wall-associated hydrolase family (DIP1621). Both enzymes are encoded by the core genome and probably contribute indirectly to adhesion of *C. diphtheriae*, as they are involved in organizing the corynebacterial cell surface (36, 55). The high degree of diversity of pilus gene clusters in *C. diphtheriae* shows that the process of adhesion could be more diverse than initially anticipated. Comparative analysis of adhesion properties of the sequenced *C. diphtheriae* strains are now necessary to experimentally detect and describe differences in adhesion to mammalian host cells. The enormous collection of variable pilus gene clusters detected in this pangenome project may reveal novel and more detailed insights into adhesion properties of *C. diphtheriae*.

ACKNOWLEDGMENTS

E.T. acknowledges the receipt of a scholarship of the CLIB Graduate Cluster Industrial Biotechnology. S.D.C.S. was supported by a CAPES-DAAD scholarship. J.B. and S.J. acknowledge funding by the German Federal Ministry of Education and Research "GenoMik-Transfer" project.

We thank Burkhard Linke (CeBiTec) for bioinformatics support. The valuable contribution of the CeBiTec sequencing team to this pangenome project is gratefully acknowledged.

REFERENCES

1. **Andrews SC, Robinson AK, Rodriguez-Quinones F.** 2003. Bacterial iron homeostasis. FEMS Microbiol. Rev. **27**:215–237.
2. **Badger JH, Olsen GJ.** 1999. CRITICA: coding region identification tool invoking comparative analysis. Mol. Biol. Evol. **16**:512–524.
3. **Barksdale WL, Pappenheimer AM, Jr.** 1954. Phage-host relationships in nontoxigenic and toxigenic diphtheria bacilli. J. Bacteriol. **67**:220–232.
4. **Blom J, et al.** 2009. EDGAR: a software framework for the comparative analysis of prokaryotic genomes. BMC Bioinformatics **10**:154.
5. **Bottacini F, et al.** 2010. Comparative genomics of the genus *Bifidobacterium.* Microbiology **156**:3243–3254.
6. **Brune I, et al.** 2006. The DtxR protein acting as dual transcriptional regulator directs a global regulatory network involved in iron metabolism of *Corynebacterium glutamicum.* BMC Genomics **7**:21.
7. **Cerdeño-Táarraga AM, et al.** 2003. The complete genome sequence and analysis of *Corynebacterium diphtheriae* NCTC13129. Nucleic Acids Res. **31**:6516–6523.
8. **Crosa JH, Walsh CT.** 2002. Genetics and assembly line enzymology of siderophore biosynthesis in bacteria. Microbiol. Mol. Biol. Rev. **66**: 223–249.
9. **D'Afonseca V, et al.** 2012. Reannotation of the *Corynebacterium diphtheriae* NCTC13129 genome as a new approach to studying gene targets connected to virulence and pathogenicity in diphtheria. Open Access Bioinformatics **4**:1–13.
10. **Darling AE, Mau B, Perna NT.** 2010. Progressive Mauve: multiple genome alignment with gene gain, loss and rearrangement. PLoS One **5**:e11147. doi:10.1371/journal.pone.0011147.
11. **Delcher AL, Harmon D, Kasif S, White O, Salzberg SL.** 1999. Improved microbial gene identification with GLIMMER. Nucleic Acids Res. **27**: 4636–4641.
12. **Dittmann S, et al.** 2000. Successful control of epidemic diphtheria in the states of the Former Union of Soviet Socialist Republics: lessons learned. J. Infect. Dis. **181**:S10–S22.
13. **Felsenstein J.** 1989. PHYLIP—Phylogeny Inference Package (version 3.2). Cladistics **5**:164–166.
14. **Finn RD, et al.** 2010. The Pfam protein families database. Nucleic Acids Res. **38**:D211–D222.
15. **Fourel G, Phalipon A, Kaczorek M.** 1989. Evidence for direct regulation of diphtheria toxin gene transcription by an Fe^{2+}-dependent DNA-binding repressor, DtoxR, in *Corynebacterium diphtheriae.* Infect. Immun. **57**:3221–3225.
16. **Fraser-Liggett CM.** 2005. Insights on biology and evolution from microbial genome sequencing. Genome Res. **15**:1603–1610.
17. **Freeman VJ.** 1951. Studies on the virulence of bacteriophage-infected strains of *Corynebacterium diphtheriae.* J. Bacteriol. **61**:675–688.
18. **Gaspar AH, Ton-That H.** 2006. Assembly of distinct pilus structures on the surface of *Corynebacterium diphtheriae.* J. Bacteriol. **188**:1526–1533.
19. **Gomes DL, et al.** 2009. *Corynebacterium diphtheriae* as an emerging pathogen in nephrostomy catheter-related infection: evaluation of traits associated with bacterial virulence. J. Med. Microbiol. **58**:1419–1427.
20. **Gordon D, Abajian C, Green P.** 1998. Consed: a graphical tool for sequence finishing. Genome Res. **8**:195–202.
21. **Griffiths E.** 1991. Iron and bacterial virulence—a brief overview. Biol. Met. **4**:7–13.
22. **Grissa I, Bouchon P, Pourcel C, Vergnaud G.** 2008. On-line resources for bacterial micro-evolution studies using MLVA or CRISPR typing. Biochimie **90**:660–668.
23. **Grissa I, Vergnaud G, Pourcel C.** 2007. CRISPRFinder: a web tool to identify clustered regularly interspaced short palindromic repeats. Nucleic Acids Res. **35**:W52–W57.
24. **Hadfield TL, McEvoy P, Polotsky Y, Tzinserling VA, Yakovlev AA.** 2000. The pathology of diphtheria. J. Infect. Dis. **181**:S116–S120.
25. **Halachev MR, Loman NJ, Pallen MJ.** 2011. Calculating orthologs in bacteria and archaea: a divide and conquer approach. PLoS One **6**:e28388. doi:10.1371/journal.pone.0028388.
26. **Hiller NL, et al.** 2007. Comparative genomic analyses of seventeen *Streptococcus pneumoniae* strains: insights into the pneumococcal supragenome. J. Bacteriol. **189**:8186–8195.
27. **Hirata R, Jr, et al.** 2004. Patterns of adherence to HEp-2 cells and actin polymerisation by toxigenic *Corynebacterium diphtheriae* strains. Microb. Pathog. **36**:125–130.

28. **Holmes RK.** 2000. Biology and molecular epidemiology of diphtheria toxin and the *tox* gene. J. Infect. Dis. **181**:S156–S167.
29. **Honma Y, et al.** 2009. A case of afebrile pneumonia caused by non-toxigenic *Corynebacterium diphtheriae.* J. Infect. Dis. **62**:327–329.
30. **Husemann P, Stoye J.** 2010. r2cat: synteny plots and comparative assembly. Bioinformatics **26**:570–571.
31. **Iwaki M, et al.** 2010. Genome organization and pathogenicity of *Corynebacterium diphtheriae* C7(−) and PW8 strains. Infect. Immun. **78**: 3791–3800.
32. **Jolley KA, Chan MS, Maiden MC.** 2004. mlstdbNet—distributed multi-locus sequence typing (MLST) databases. BMC Bioinformatics **5**:86.
33. **Kalinowski J, et al.** 2003. The complete *Corynebacterium glutamicum* ATCC 13032 genome sequence and its impact on the production of L-aspartate-derived amino acids and vitamins. J. Biotechnol. **104**:5–25.
34. **Kitchin NR.** 2011. Review of diphtheria, tetanus and pertussis vaccines in clinical development. Expert Rev. Vaccines **10**:605–615.
35. **Klebs E.** 1883. Ueber Diphtherie. Verh. Kongr. Innere Med. **2**:139–154.
36. **Kolodkina V, Denisevich T, Titov L.** 2011. Identification of *Corynebacterium diphtheriae* gene involved in adherence to epithelial cells. Infect. Genet. Evol. **11**:518–521.
37. **Kunkle CA, Schmitt MP.** 2005. Analysis of a DtxR-regulated iron transport and siderophore biosynthesis gene cluster in *Corynebacterium diphtheriae.* J. Bacteriol. **187**:422–433.
38. **Kunkle CA, Schmitt MP.** 2003. Analysis of the *Corynebacterium diphtheriae* DtxR regulon: identification of a putative siderophore synthesis and transport system that is similar to the *Yersinia* high-pathogenicity island-encoded yersiniabactin synthesis and uptake system. J. Bacteriol. **185**: 6826–6840.
39. **Larkin MA, et al.** 2007. Clustal W and Clustal X version 2.0. Bioinformatics **23**:2947–2948.
40. **Leong D, Murphy JR.** 1985. Characterization of the diphtheria tox transcript in *Corynebacterium diphtheriae* and *Escherichia coli.* J. Bacteriol. **163**:1114–1119.
41. **Lerat E, Daubin V, Moran NA.** 2003. From gene trees to organismal phylogeny in prokaryotes: the case of the gamma-Proteobacteria. PLoS Biol. **1**:E19. doi:10.1371/journal.pbio.0000019.
42. **Linke B, McHardy AC, Neuweger H, Krause L, Meyer F.** 2006. REGANOR: a gene prediction server for prokaryotic genomes and a database of high quality gene predictions for prokaryotes. Appl. Bioinformatics **5**:193–198.
43. **Loeffler F.** 1884. Untersuchung über die Bedeutung der Mikroorganismen für die Entstehung der Diphtherie. Mitt. Kaiserl. Gesundheitsamt **2**:421–499.
44. **Lukjancenko O, Wassenaar TM, Ussery DW.** 2010. Comparison of 61 sequenced *Escherichia coli* genomes. Microb. Ecol. **60**:708–720.
45. **Mandlik A, Das A, Ton-That H.** 2008. The molecular switch that activates the cell wall anchoring step of pilus assembly in gram-positive bacteria. Proc. Natl. Acad. Sci. U. S. A. **105**:14147–14152.
46. **Mandlik A, Swierczynski A, Das A, Ton-That H.** 2007. *Corynebacterium diphtheriae* employs specific minor pilins to target human pharyngeal epithelial cells. Mol. Microbiol. **64**:111–124.
47. **Mattos-Guaraldi AL, Cappelli EA, Previato JO, Formiga LC, Andrade AF.** 1999. Characterization of surface saccharides in two *Corynebacterium diphtheriae* strains. FEMS Microbiol. Lett. **170**:159–166.
48. **Medini D, Donati C, Tettelin H, Masignani V, Rappuoli R.** 2005. The microbial pan-genome. Curr. Opin. Genet. Dev. **15**:589–594.
49. **Meyer F, et al.** 2003. GenDB—an open source genome annotation system for prokaryote genomes. Nucleic Acids Res. **31**:2187–2195.
50. **Mishra B, Dignan RJ, Hughes CF, Hendel N.** 2005. *Corynebacterium diphtheriae* endocarditis—surgery for some but not all! Asian Cardiovasc. Thorac. Ann. **13**:119–126.
51. **Mokrousov I, Limeschenko E, Vyazovaya A, Narvskaya O.** 2007. *Corynebacterium diphtheriae* spoligotyping based on combined use of two CRISPR loci. Biotechnol. J. **2**:901–906.
52. **Nagarkar PP, Ravetkar SD, Watve MG.** 2002. The amino acid requirements of *Corynebacterium diphtheriae* PW 8 substrain CN 2000. J. Appl. Microbiol. **92**:215–220.
53. **Nyström T.** 2004. Growth versus maintenance: a trade-off dictated by RNA polymerase availability and sigma factor competition? Mol. Microbiol. **54**:855–862.
54. **Oram DM, Avdalovic A, Holmes RK.** 2004. Analysis of genes that encode DtxR-like transcriptional regulators in pathogenic and saprophytic corynebacterial species. Infect. Immun. **72**:1885–1895.
55. **Ott L, et al.** 2010. *Corynebacterium diphtheriae* invasion-associated protein (DIP1281) is involved in cell surface organization, adhesion and internalization in epithelial cells. BMC Microbiol. **10**:2.
56. **Park WH, Williams AW.** 1896. The production of diphtheria toxin. J. Exp. Med. **1**:164–185.
57. **Petersen TN, Brunak S, von Heijne G, Nielsen H.** 2011. SignalP 4.0: discriminating signal peptides from transmembrane regions. Nat. Methods **8**:785–786.
58. **Pimenta FP, Hirata R, Jr, Rosa AC, Milagres LG, Mattos-Guaraldi AL.** 2008. A multiplex PCR assay for simultaneous detection of *Corynebacterium diphtheriae* and differentiation between non-toxigenic and toxigenic isolates. J. Med. Microbiol. **57**:1438–1439.
59. **Rappuoli R, Michel JL, Murphy JR.** 1983. Integration of corynebacteriophages β^{tox+}, ω^{tox+}, and γ^{tox-} into two attachment sites on the *Corynebacterium diphtheriae* chromosome. J. Bacteriol. **153**:1202–1210.
60. **Rappuoli R, Michel JL, Murphy JR.** 1983. Restriction endonuclease map of corynebacteriophage $\gamma_{c}{}^{tox+}$ isolated from the Park-Williams no. 8 strain of *Corynebacterium diphtheriae.* J. Virol. **45**:524–530.
61. **Ratti G, Covacci A, Rappuoli R.** 1997. A $\text{tRNA}_2{}^{\text{Arg}}$ gene of *Corynebacterium diphtheriae* is the chromosomal integration site for toxinogenic bacteriophages. Mol. Microbiol. **25**:1179–1181.
62. **Rogers EA, Das A, Ton-That H.** 2011. Adhesion by pathogenic corynebacteria. Adv. Exp. Med. Biol. **715**:91–103.
63. **Salyers AA, Amabile-Cuevas CF.** 1997. Why are antibiotic resistance genes so resistant to elimination? Antimicrob. Agents Chemother. **41**: 2321–2325.
64. **Schneider J, et al.** 2010. CARMEN—Comparative Analysis and in silico Reconstruction of organism-specific MEtabolic Networks. Genet. Mol. Res. **9**:1660–1672.
65. **Schröder J, et al.** 2012. Complete genome sequence, lifestyle, and multi-drug resistance of the human pathogen Corynebacterium resistens DSM 45100 isolated from blood samples of a leukemia patient. BMC Genomics **13**:141.
66. **Shapiro JA.** 1979. Molecular model for the transposition and replication of bacteriophage Mu and other transposable elements. Proc. Natl. Acad. Sci. U. S. A. **76**:1933–1937.
67. **Skarstad K, Bernander R, Boye E.** 1995. Analysis of DNA replication *in vivo* by flow cytometry. Methods Enzymol. **262**:604–613.
68. **Soares SC, et al.** 2012. PIPS: pathogenicity island prediction software. PLoS One 7:e30848. doi:10.1371/journal.pone.0030848.
69. **Suzek BE, Ermolaeva MD, Schreiber M, Salzberg SL.** 2001. A probabilistic method for identifying start codons in bacterial genomes. Bioinformatics **17**:1123–1130.
70. **Swaminathan A, et al.** 2007. Housekeeping sortase facilitates the cell wall anchoring of pilus polymers in *Corynebacterium diphtheriae.* Mol. Microbiol. **66**:961–974.
71. **Swierczynski A, Ton-That H.** 2006. Type III pilus of corynebacteria: pilus length is determined by the level of its major pilin subunit. J. Bacteriol. **188**:6318–6325.
72. **Tamura K, Dudley J, Nei M, Kumar S.** 2007. MEGA4: Molecular Evolutionary Genetics Analysis (MEGA) software version 4.0. Mol. Biol. Evol. **24**:1596–1599.
73. **Tao X, Schiering N, Zeng HY, Ringe D, Murphy JR.** 1994. Iron, DtxR, and the regulation of diphtheria toxin expression. Mol. Microbiol. **14**: 191–197.
74. **Terns MP, Terns RM.** 2011. CRISPR-based adaptive immune systems. Curr. Opin. Microbiol. **14**:321–327.
75. **Tettelin H, et al.** 2005. Genome analysis of multiple pathogenic isolates of *Streptococcus agalactiae*: implications for the microbial "pan-genome." Proc. Natl. Acad. Sci. U. S. A. **102**:13950–13955.
76. **Tettelin H, et al.** 2001. Complete genome sequence of a virulent isolate of *Streptococcus pneumoniae.* Science **293**:498–506.
77. **Tettelin H, Riley D, Cattuto C, Medini D.** 2008. Comparative genomics: the bacterial pan-genome. Curr. Opin. Microbiol. **11**:472–477.
78. **Ton-That H, Schneewind O.** 2003. Assembly of pili on the surface of *Corynebacterium diphtheriae.* Mol. Microbiol. **50**:1429–1438.
79. **Trost E, et al.** 2011. Comparative analysis of two complete *Corynebacterium ulcerans* genomes and detection of candidate virulence factors. BMC Genomics **12**:383.
80. **Trost E, et al.** 2010. The complete genome sequence of *Corynebacterium*

pseudotuberculosis FRC41 isolated from a 12-year-old girl with necrotizing lymphadenitis reveals insights into gene-regulatory networks contributing to virulence. BMC Genomics **11**:728.

81. **Ventura M, et al.** 2007. Genomics of *Actinobacteria*: tracing the evolutionary history of an ancient phylum. Microbiol. Mol. Biol. Rev. **71**:495–548.
82. **Viguetti SZ, et al.** 2012. Multilocus sequence types of invasive *Corynebacterium diphtheriae* isolated in the Rio de Janeiro urban area, Brazil. Epidemiol. Infect. **140**:617–620.
83. **Vitek CR.** 2006. Diphtheria. Curr. Top. Microbiol. Immunol. **304**:71–94.
84. **von Behring EA.** 1893. Zur Behandlung der Diphtherie mit Diphtherieheilserum. Dtsch. Med. Wochenschr. **23**:543–547.
85. **von Graevenitz A, Bernard K.** 2006. The genus *Corynebacterium*—medical, p 819–842. *In* Dworkin M, Falkow F, Rosenberg E, Schleifer KH, Stackebrandt E (ed), The prokaryotes, 3rd ed, vol 3. Springer, New York, NY.
86. **Yukawa H, et al.** 2007. Comparative analysis of the *Corynebacterium glutamicum* group and complete genome sequence of strain R. Microbiology **153**:1042–1058.